N7526475

TECHNICAL REPORT STANDARD TITLE PAGE

1. Report No. NASA CR-ERIM 109600-16-F	2. Government Accession No.	3. Recipient's Catalog No.
4. Title and Subtitle METHODS OF EXTENDING SIGNATURES AND TRAINING WITHOUT GROUND INFORMATION		5. Report Date May 1975 6. Performing Organization Code
7. Author(s) R.G. Henderson, G.S. Thomas, and R.F. Nalepka Infrared and Optics Division		8. Performing Organization Report No. 109600-16-F
9. Performing Organization Name and Address Environmental Research Institute of Michigan P. O. Box 618 Ann Arbor, Michigan 48107		10. Work Unit No. Task II 11. Contract or Grant No. NAS9-14123
12. Sponsoring Agency Name and Address National Aeronautics and Space Administration Lyndon B. Johnson Space Center Earth Observations Division Houston, Texas 77058		13. Type of Report and Period Covered Final Technical Report 15 May 1974 through 14 March 1975 14. Sponsoring Agency Code

15. Supplementary Notes

Dr. Andrew E. Potter is Technical Monitor for NASA/JSC.

16. Abstract

Methods of performing signature extension, using LANDSAT-1 data, are explored. The emphasis is on improving the performance and cost-effectiveness of large area wheat surveys. Two new methods were developed -- ASC, and MASC. Two methods, Ratio, and RADIFF, previously used with aircraft data were adapted to and tested on LANDSAT-1 data. Included in this study was an investigation into the sources and nature of between scene data variations.

Initial investigations into the selection of training fields without in situ ground truth were undertaken.

REPRODUCED BY: NTIS
U.S. Department of Commerce
National Technical Information Service
Springfield, Virginia 22161

17. Key Words	18. Distribution Statement
Remote Sensing Multispectral Scanning Multispectral Data Collection Large-Area Surveys Signature Extension	Initial distribution is indicated at the end of this document.

19. Security Classif. (of this report)	20. Security Classif. (of this page)	21. No. of Pages	22. Price
Unclassified	Unclassified	91	

PREFACE

This report describes part of a comprehensive and continuing program of research in multispectral remote sensing of the environment from aircraft and satellites and the supporting effort of ground-based researchers in recording, coordinating, and analyzing the data gathered by these means. The basic objective of this program is to improve the utility of remote sensing as a tool for providing decision makers with timely and economical information from large geographical areas.

The feasibility of using remote sensing techniques to detect and discriminate between objects or conditions at or near the surface of the earth has been demonstrated. Applications in agriculture, urban planning, water quality control, forest management, and other areas have been developed. The thrust of this program is directed toward the development and improvement of advanced remote sensing systems and includes assisting in data collection, processing and analysis, and ground truth verification .

The research covered in this report was performed under NASA Contract NAS9-14123. The program was directed by R. R. Legault, Director of ERIM's Infrared and Optics Division and an Institute Vice-President, and J. D. Erickson, Head of Information Systems and Analysis Department. The institute number for this report is 109600-16-F.

The authors wish to acknowledge the administrative direction provided by Mr. R. R. Legault and Dr. Jon D. Erickson and the technical assistance given by Mr. W. W. Pillars. Ms . D. Dickerson, L. Parker, and G. Sotomayor are thanked for their secretarial assistance.

CONTENTS

FIGURES

FIGURES (Cont.)

TABLES

1
INTRODUCTION

With the development of satellite multispectral scanners (MSS) it has become possible to gather data from large areas. This data collection effort has the potential of providing timely information concerning the state of world-wide crop production. In order that this potential is realized it is necessary to find methods of processing the data in a timely and cost effective manner.

A major stumbling block in the way of achieving cost effective processing is the requirement of large amounts of ground information. This ground information is required to train the computer to recognize different crop types. Because of variations in measurement conditions when the data is collected the computer must be retrained on a regular basis. The crop signatures are not constant in either time or space. The need to retrain the computer requires new ground information which is both costly and time consuming.

The first objective of this investigation is to develop signature extension techniques which will allow the crop signatures to be updated or corrected for variations in the measurement conditions so that signatures derived from the training data set (TDS)* can be successfully used for recognition on a different, removed, recognition data set (RDS). This objective can be accomplished using the following approaches:

1) Extract signatures from the TDS and then find a transformation which will map those signatures onto the RDS. The transformation will correct for the differing measurement conditions of the two data sets .

2) Preprocess the two data sets to remove the effects of the varying measurement conditions and then extract signatures from the TDS and apply them to the RDS.

*Appendix IV lists the abbreviations used in this report.

We will call these two signature extension methods Type 1 and Type 2, respectively.

In this report we will examine the sources of variation in the data and two Type 1 and two Type 2 methods for correcting for those variations. The Type 1 methods are the ASC and MASC algorithms which are discussed in sections 5.1 and 5.2 respectively. The Type 2 methods are Ratios and RADIFF. These are discussed in sections 6.1 and 6.2. In section 7 we will discuss the results of an experiment to determine the possible effects on recognition of variation in atmospheric state and scanner view angle.

While the signature extension methods which we examine in this report are applied to single pass data the general approaches can also be used to extend multitemporal signatures. In the future some of the methods developed here will be extended for use on multitemporal data sets.

The second objective of this study is to investigate methods of defining training fields without in situ ground information. If training fields can be identified without the use of ground information then locally derived signatures may be used for the recognition of every data set. In section 8 we discuss some preliminary investigations into this problem.

2
SUMMARY

Investigations into the sources and nature of between-scene data variations were carried out. The variations in the data were seen to be due to three types of variations in the measurement conditions. These were:

1. Instrumental,
2. Environmental,
3. On the Ground Changes.

These variations in measurement conditions were responsible for multiplicative and additive variations in the crop signatures when going from one data set to another.

In order to correct for varying measurement conditions four signature extension methods were developed and tested. The four were:

1. ASC,
2. MASC,
3. Ratio of Spectral Bands,
4. RADIFF.

Each method was, in theory, capable of correcting for a subset of the possible variations in measurement conditions.

The four methods were tested on LANDSAT-1 data that was collected for the CITARS project. Of the four methods the ASC and MASC algorithms performed the best. MASC showed the most promise as a signature extension technique and as a tool for further investigating the nature of the inter-scene data variations.

Initial investigations into defining training fields without the aid of ground information have been carried out. These investigations have been based on the attempt to define regions of the data space which are occupied by single crop types. To aid this attempt two methods of transforming a region from one data set's space to another data set's space were developed. The methods are:

1. Overlay Method,
2. Method of Affine Transformations.

The work in this area is at too early a stage of development to be able to make any judgements as to the best method of defining the regions in the data space that are associated with particular crop types.

3
SOURCES OF DATA VARIABILITY

In order that we can develop methods to correct for variations in the data between the TDS and RDS we must investigate the source of those variations.

There are a number of factors which can be sources of variation in scanner signals. Some of these sources are listed below, where we have divided them into three categories: instrumental sources, environmental sources, and scene related sources of variation.

SOURCES OF VARIATION IN MULTISPECTRAL SCANNER SIGNALS

A. Instrument
   - Scanner Electronics and recorder instabilities
   - Gain changes
   - Nonuniform angular responsivity

B. Environment
   - Changes in irradiance
   - Changes in atmospheric transmittance
   - Changes in atmospheric path radiance

C. Scene
   - Geometric effects
   - Reflectance effects

Instrumental sources are associated with the mechanics, optics, and electronics of the multispectral scanner. Included in this category are gain changes, non-uniform angular responsivity, and other recorder and electronic instabilities. Since many of these effects are deterministic, they can be eliminated from the data during an initial data preparation stage.

Environmental sources of variation include changes in the magnitude and spectral make-up of the irradiance at ground level, changes in atmospheric transmittance, and changes in path radiance. Changes in irradiance result from changes in the atmospheric state as well as from solar positional changes that occur between the times the data sets are collected.

Atmospheric transmittance and path radiance will also change as the atmospheric state changes . These quantities are also functions of scan angle since they depend on the path length from the ground to the scanner. In Fig. 1 we see the variation of path radiance, as calculated using the ERIM Radiative Transfer Model [1], for different atmospheres (as represented by visibility). It is clear that path radiance can vary considerably with changing atmospheric state, up to 37% for the visibilities shown in Fig. 1. Shown in Table 1 is the effect of scan angle on both the path radiance and total radiance received by a scanner. The change in path radiance over a range of scanner view angles, from $+6^{o}$ to -6^{o} relative to nadir, is greater than 18%. The change in total radiance, over the same range of view angles, can be as large as 10%.

The in-scene effects are of two types. The first effect is the geometric variations due to sun-angle and bidirectional reflectance. These will cause the amount of radiation reflected in a particular direction to depend on time of day and position of the target in the scene. The other in-scene effect is variation in target reflectance. This may be caused by differences in moisture content of the soil or soil type. Also differences in irrigation and fertilization or crop vigor will cause variation in the crop reflectances.

To see how these effects combine to affect the variability of the MSS signals we write the equation for the signal recorded by the scanner in channel i for crop α,

$$S_{\alpha}^{(i)} = G^{(i)}E^{(i)}T^{(i)}\rho_{\alpha}^{(i)} + G^{(i)}L_{p}^{(i)} \quad . \tag{1}$$

The instrumental effects are contained in the gain term $G^{(i)}$, while the atmospheric effects are contained in the irradiance $E^{(i)}$, the transmittance $T^{(i)}$, and the path radiance $L_{p}^{(i)}$. The in-scene effects are contained in the reflectance $\rho_{\alpha}^{(i)}$. Thus, the effect of variations in atmosphere and

[1] Robert E. Turner, "Radiative Transfer in Real Atmospheres", ERIM Report No. 190100-24-T, December 1973.

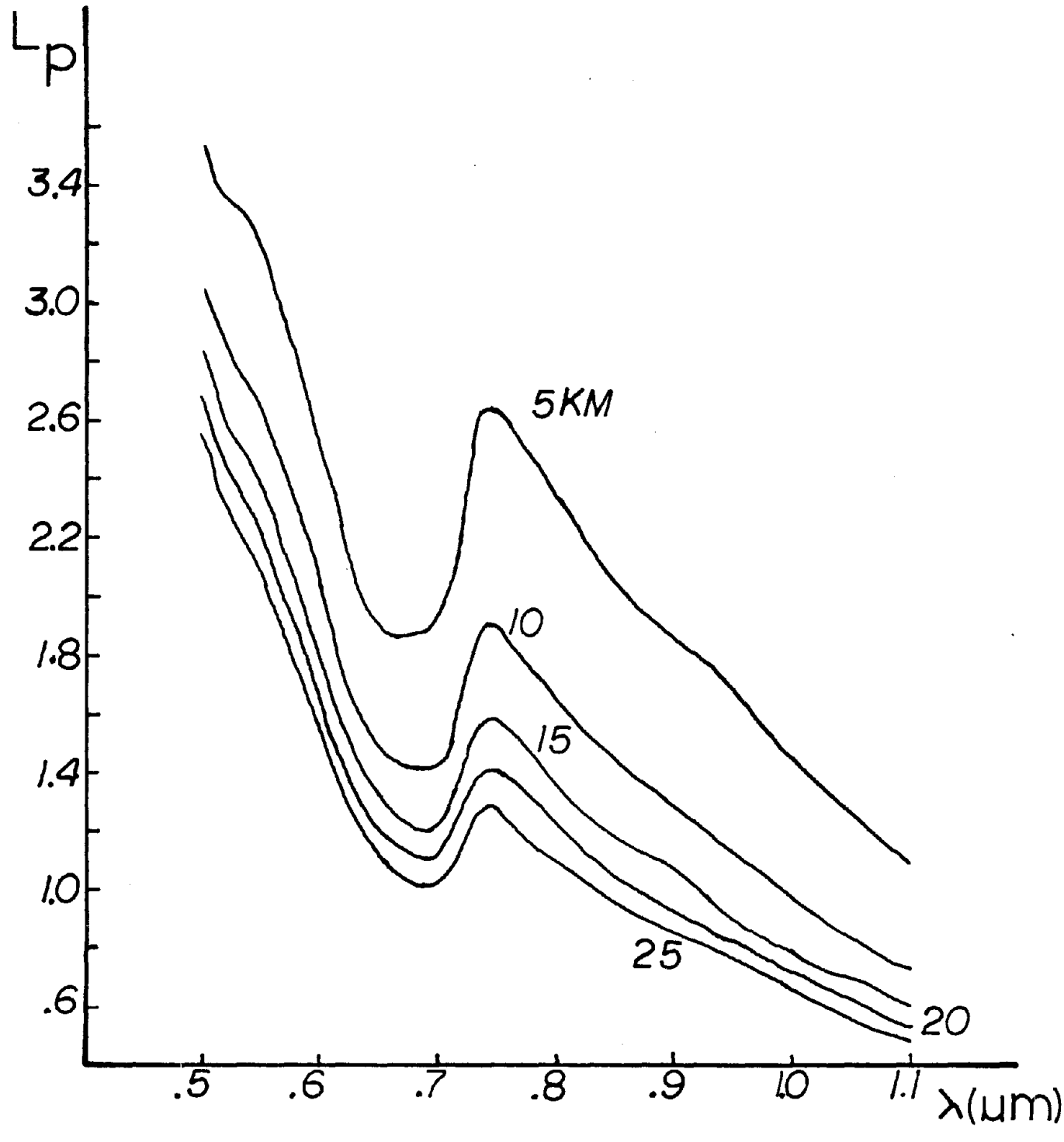

FIGURE 1. DEPENDENCE OF PATH RADIANCE AS A FUNCTION OF WAVELENGTH FOR SEVERAL VISIBILITIES. Altitude = 910 km, Solar Zenith = 62°, Green Vegetation Target on Green Vegetation Background. (Calculation based on ERIM Radiative Transfer Model)

TABLE 1. SCAN ANGLE EFFECTS ATTRIBUTABLE TO THE ATMOSPHERE

Azimuth Relative to Sun, ϕ	Scan Angle Relative to Nadir θ	Spectral Radiances* ($mW/cm^2 \cdot sr \cdot \mu m$) λ = 0.55 μm Path	λ = 0.55 μm Total	λ = 0.75 μm Path	λ = 0.75 μm Total
38°	(-) 6°	2.51	4.70	0.98	2.78
	0°	2.71	4.90	1.06	2.86
218°	6°	2.98	5.17	1.17	2.96

Percent Change From Nadir (θ=0°) Value

ϕ	θ	λ = 0.55 μm Path	λ = 0.55 μm Total	λ = 0.75 μm Path	λ = 0.75 μm Total
38°	(-) 6°	-7.3	-4.2	-7.2	-2.8
	0°	0	0	0	0
218°	6°	10.2	5.5	10.1	3.7

Percent Change From One Side of Nadir To Other

Scan Angle Change	λ = 0.55 μm Path	λ = 0.55 μm Total	λ = 0.75 μm Path	λ = 0.75 μm Total
-6° to + 6°	18.9	10.1	18.7	6.6

*Target Reflectance = Background Albedo = 8%
Solar Zenith Angle = 39°
Optical Thickness of Atmosphere = 0.3812 for 0.55 μm and 0.2854 for 0.75 μm.

instrumental response is to produce both multiplicative and additive variations in the recorded signal. The in-scene variations will produce multiplicative variations in the scanner signal.

In this report we investigate a number of approaches to remove these variations. The ASC method produces an additive signature correction and is thus primarily concerned with variations in path radiance. The MASC algorithm produces both an additive and multiplicative signature correction. It is thus potentially capable of correcting for all of the variations we have discussed, however, variations in the reflectances can only be corrected for in an average way. The Ratios of Spectral Bands method can correct for all multiplicative variations if they are correlated between channels and if the path radiances are negligible. The RADIFF method removes from the Ratio method the restriction that the path radiance be negligible.

4
DESCRIPTION OF DATA

The data sets used in this study were originally designed for the CITARS [2] project. They consisted of a number of 8 km x 32 km sites in Indiana and Illinois collected by LANDSAT-1* during the 1973 growing season. In particular the data sets Fayette Co., Illinois, June 10, June 11, and August 21; Shelby Co., Indiana, June 8; and White Co., Indiana, August 21 were employed.

For the June period the Fayette, June 11 (F6-11) data set was arbitrarily defined as the training data set (TDS). The Shelby, June 8 (S6-8) and Fayette, June 10 (F6-10) were chosen as the recognition data sets (RDS). For the August period White, August 21 (W8-21) was defined to be the TDS while Fayette, August 21 (F8-21) was chosen as the RDS.

For the CITARS study certain fields of each site were chosen for training and others were designated as test fields. In our TDS, signatures were extracted from the CITARS designated training fields while all fields in the RDS (i.e., both training and test) were used to test the recognition performance of the various signature extension methods. The results of the recognition experiments are described in terms of field-center pixel recognition and confusion of the major crops. Field-center pixel recognition performance was used to evaluate the techniques rather than crop proportion estimation because the objective of signature extension is the mapping of class spectral information from one data set to another. Proportion estimation depends on the correct recognition of impure boundary pixels and is therefore a function of the type of classifier used. During June the major

[2] W. A. Malila, D. P. Rice and R. C. Cicone, "Final Report on the CITARS Effort by the Environmental Research Institute of Michigan", ERIM Report No. 109600-12-F, February 1975.

*The LANDSAT-1 MSS bands are numbered 4,5,6,7, in this report we have renumbered them as channels 1,2,3,4.

crop was wheat and the results are reported as percent correct wheat recognition and percent correct "other" recognition. Actually "other" crops were considered correctly recognized if they were classified as anything other than wheat. Using this definition of "correct other", we could leave everything unclassified and have 100% "correct other". For this reason the "percent other correct" results may be somewhat misleading in terms of evaluating the value of a particular signature extension method. During the August period corn and soybeans were the major crops . The "percent other correct" has the same meaning as for the June period.

One change was implemented in the June Fayette data sets. The original test field designated 29-29 was labeled as being all wheat. Investigations into the datum values as well as the photo-imagery led to the conclusion that field 29-29 was in fact three separate fields. The middle field was determined to be wheat and the coordinates of field 29-29 were adjusted to include the central ten pixels.

The signatures, for this investigation, were extracted from each of the training fields in the TDS and then were combined on the basis of ground information concerning the crops of each training field. Thus the field signatures from every wheat training field were combined, using a χ^2 rejection test, to form a wheat crop signature. The χ^2 rejection test was based on a final χ^2 distance rejection threshold corresponding to a .001 probability of false rejection under the assumption of normality and four degrees of freedom. This resulted in rather large signature covariances and a smaller χ^2 level may have produced better signatures. As it was, two wheat modes remained apparent and a second wheat signature, designated "wheat 2", was produced. The signature set used during the June period included: wheat, wheat 2, water, trees, bare soil, and weeds.

For the August period, the signatures from W8-21 were formed in a similar manner to the F6-11 signatures. The only difference is in the χ^2 rejection level used when combining the individual field signatures. The final χ^2 distance rejection threshold corresponded to a .01 probability of

false rejection. The August signatures used were: corn, soybeans, pasture, quarry, and trees.

Recognition was performed on the RDS using the ERIM Linear Classifier [3]. A null test threshold corresponding to a .001 χ^2 probability was used. Thus each pixel was classified into one of (n+1) bins where n was the number of signatures. Non-major crops put in the unclassified bin were considered to have been correctly classified.

[3] R. B. Crane, W. Richardson, R. H. Hieber and W. A. Malila, "A Study of Techniques for Processing Multispectral Scanner Data", ERIM Report No. 31650-155-T, September 1973.

5
TYPE 1 SIGNATURE EXTENSION METHODS

As described in the introduction (section 1) a Type 1 method is one which produces a mapping of the TDS signatures onto the RDS. This mapping may account for some or all of the inter-scene variability which exists between the TDS and RDS. In this report we investigate two Type 1 methods: ASC (additive signature correction), and MASC (multiplicative and additive signature correction). Both methods have performed reasonably well on the data sets tested.

5.1 ASC

The equation for the signal recorded by the scanner in channel i for crop α is (see discussion after equation (1)):

$$S_{\alpha}^{(i)} = G^{(i)}E^{(i)}T^{(i)}\rho_{\alpha}^{(i)} + G^{(i)}L_{p}^{(i)} .$$

If we use subscripts 1, and 2 to denote the TDS and RDS, respectively, the crop signature for the RDS can be related to the TDS crop signature by

$$S_{\alpha 2}^{(i)} = A_{\alpha}^{(i)}S_{\alpha 1}^{(i)} + B_{\alpha}^{(i)} .$$

We have defined

$$A_{\alpha}^{(i)} \equiv \frac{G_2^{(i)}E_2^{(i)}T_2^{(i)}\rho_{\alpha 2}^{(i)}}{G_1^{(i)}E_1^{(i)}T_1^{(i)}\rho_{\alpha 1}^{(i)}} , \qquad (2)$$

and

$$B_{\alpha}^{(i)} = G_2^{(i)}L_{p2}^{(i)} - A_{\alpha}^{(i)}G_1^{(i)}L_{p1}^{(i)} . \qquad (3)$$

While $E^{(i)}$, $T^{(i)}$, and $L_p^{(i)}$ all depend on atmospheric conditions, it is apparent that different L_p's for two data sets amounts to a change in the reference level with respect to which the radiance measurements of the target are made. Thus for signatures obtained from the TDS the means of the various crops may be translated up or down compared to the crop means in the RDS. If we assume that $G^{(i)}$, $E^{(i)}$, $T^{(i)}$ and $\rho_\alpha^{(i)}$ are the same for both data sets, or more precisely that

$$A_\alpha^{(i)} = \frac{G_2^{(i)} E_2^{(i)} T_2^{(i)} \rho_{\alpha 2}^{(i)}}{G_1^{(i)} E_1^{(i)} T_1^{(i)} \rho_{\alpha 1}^{(i)}} = 1, \tag{4}$$

then the TDS signatures may be extended to the RDS by finding the appropriate translation. That is

$$S_{\alpha 2}^{(i)} = S_{\alpha 1}^{(i)} + B^{(i)} ,$$

note that under the assumption of equation (4) $B^{(i)}$ is independent of the crop type α.

To examine the validity of equation (4) we plot the F6-11 signature means versus signature means obtained from F6-10 (Figure 2) and versus signature means from S6-8 (Figure 3). In figures 2 and 3 the dashed lines are the equation

$$L_{\alpha 1}^{(i)} = L_{\alpha 2}^{(i)} ;$$

the solid line is a lease square fit of the equation

$$L_{\alpha 1}^{(i)} = L_{\alpha 2}^{(i)} - B^{(i)}$$

to the data. We see that for F6-10 equation (4) holds quite well but for S6-8 the assumption is not as good. From the figures we can estimate the amount of translation required to extend the F6-11 signatures to F6-10 and S6-8. The values of $B^{(i)}$ obtained from the fitted lines in the figures are listed in table 2.

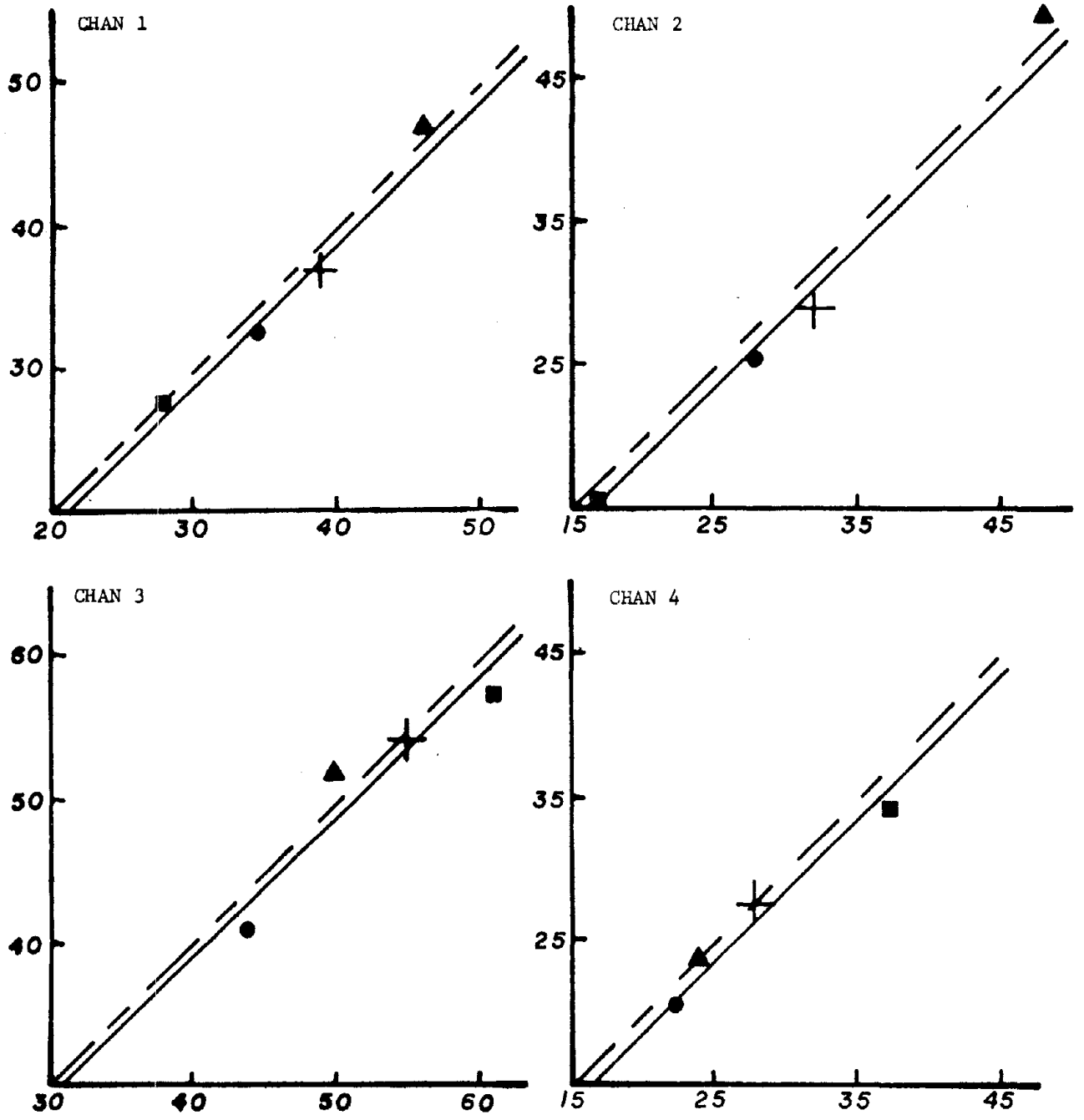

Figure 2. Plot of F6-11 Signatures vs. F6-10 Signatures, ■ -Trees, ● -Wheat, ▲ -Bare, + -Weeds, —— $L_{\alpha 1}^{(i)} = L_{\alpha 2}^{(i)} - B^{(i)}$ — — — $L_{\alpha 1}^{(i)} = L_{\alpha 2}^{(i)}$

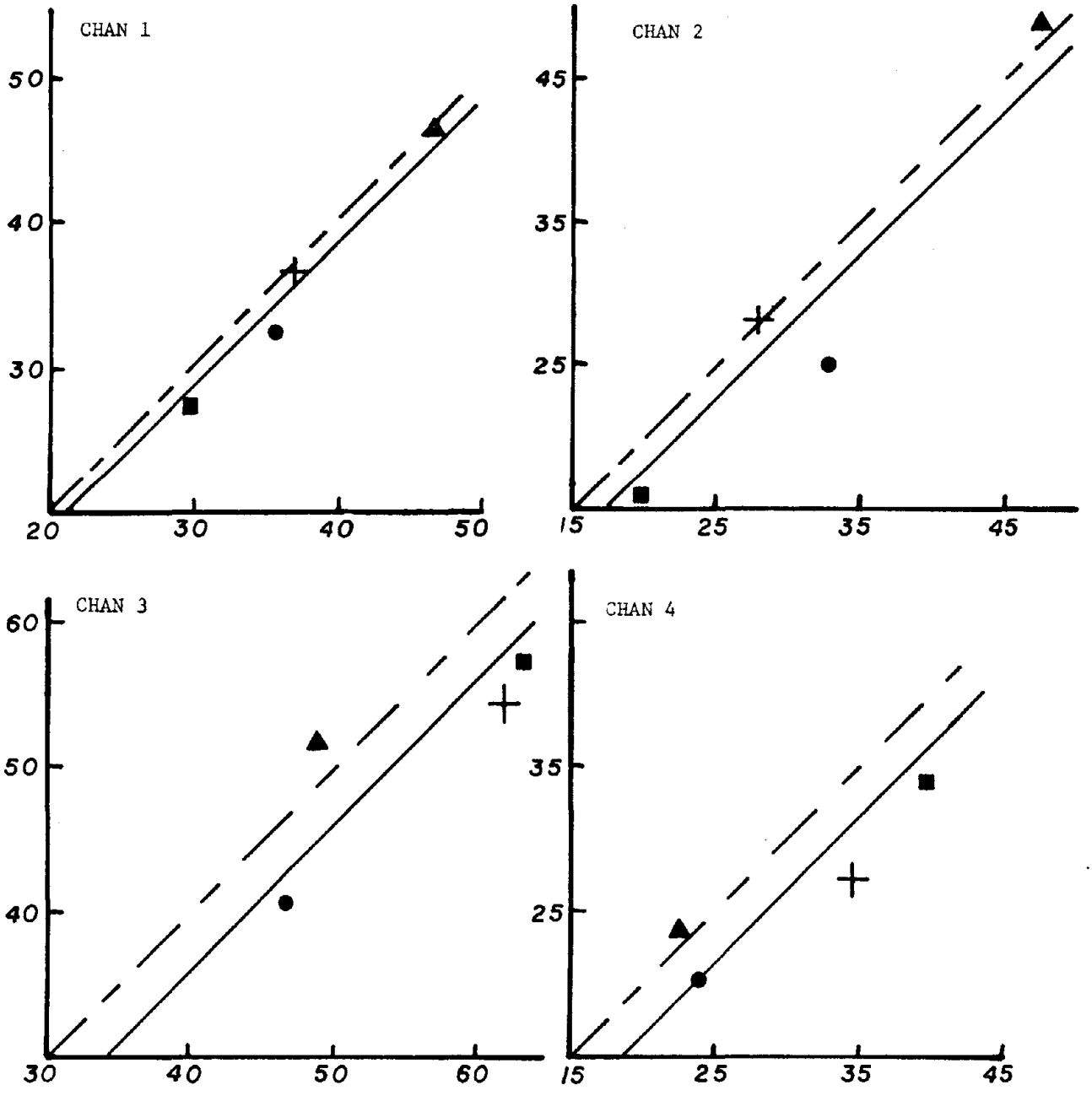

Figure 3. Plot of F6-11 Signatures vs S6-8 Signatures. ■-Trees, ●-Wheat, ▲-Bare, ✚-Weeds, ——— $L_{\alpha 1}^{(i)} = L_{\alpha 2}^{(i)} - B^{(i)}$, —— – —— $L_{\alpha 1}^{(i)} = L_{\alpha 2}^{(i)}$.

TABLE 2. TRANSLATION VECTORS FOR EXTENDING F6-11 SIGNATURES TO F6-10 AND S6-8. Values from Figures 2 and 3

Channel i	F6-11 → F6-10 $B^{(i)}$	F6-11 → S6-8 $B^{(i)}$
1	+1	+1
2	+1	+1
3	+1	+2
4	+1	+2

The values of $B^{(i)}$ in Table 2 are not of any use for signature extension since it was necessary to use ground information from F6-10 and S6-8 to obtain them. This, of course, is not the objective of signature extension. A different method must be found to estimate the translation vectors $B^{(i)}$. We recall from equation (3),

$$B^{(i)} = G_2^{(i)} L_{p2}^{(i)} - G_1^{(i)} L_{p1}^{(i)} ,$$

(using eq. (2) and (4)), that the translation vector is just the difference between the recorded path radiance of the two data sets. Thus if the gains and path radiances were known the vectors could be calculated. To find the path radiances, a model, such as the ERIM Radiative Transfer Model, could be used with measured atmospheric inputs.

In the absense of atmospheric inputs it is necessary to get information concerning the relative magnitudes of the path radiances from the two data sets. One method of doing this would be to search both the TDS and RDS for the darkest objects in each channel. However, even if in one data set the darkest object had zero reflectance, so that all of the radiation received by the

scanner was path radiance, in the other data set no such object may exist. In order to try to avoid the problem that isolated dark objects may correspond to different targets in the two data sets, the dark objects whose scanner values lie at the bottom of the histogram continuum are used. By choosing the dark objects in this way we are using more information than is contained in the data value alone. The dark object is determined by its relationship to the majority of other targets in the scene. To illustrate this we have constructed a hypothetical histogram of the scanner values in a single channel. In Figure 4 is shown the lower portion of the histogram. The value which is chosen to represent the dark object from this histogram is 13. Denoting the dark object by DO we empirically estimate the translation vectors by

$$B^{(i)} = DO_2^{(i)} - DO_1^{(i)} .$$

Using this method for extending from F6-11 to F6-10 and S6-8 yields the translation vectors listed in Table 3.

TABLE 3. TRANSLATION VECTORS OBTAINED USING DARK OBJECT SEARCH

Channel i	F6-11 → F6-10 $B^{(i)}$	F6-11 → S6-8 $B^{(i)}$
1	2	4
2	0	4
3	1	-1
4	0	0

The results of using the ASC method to extend signatures for recognition are shown in Table 4. Also listed, for comparison, are the results of using untransformed (UT) signatures.

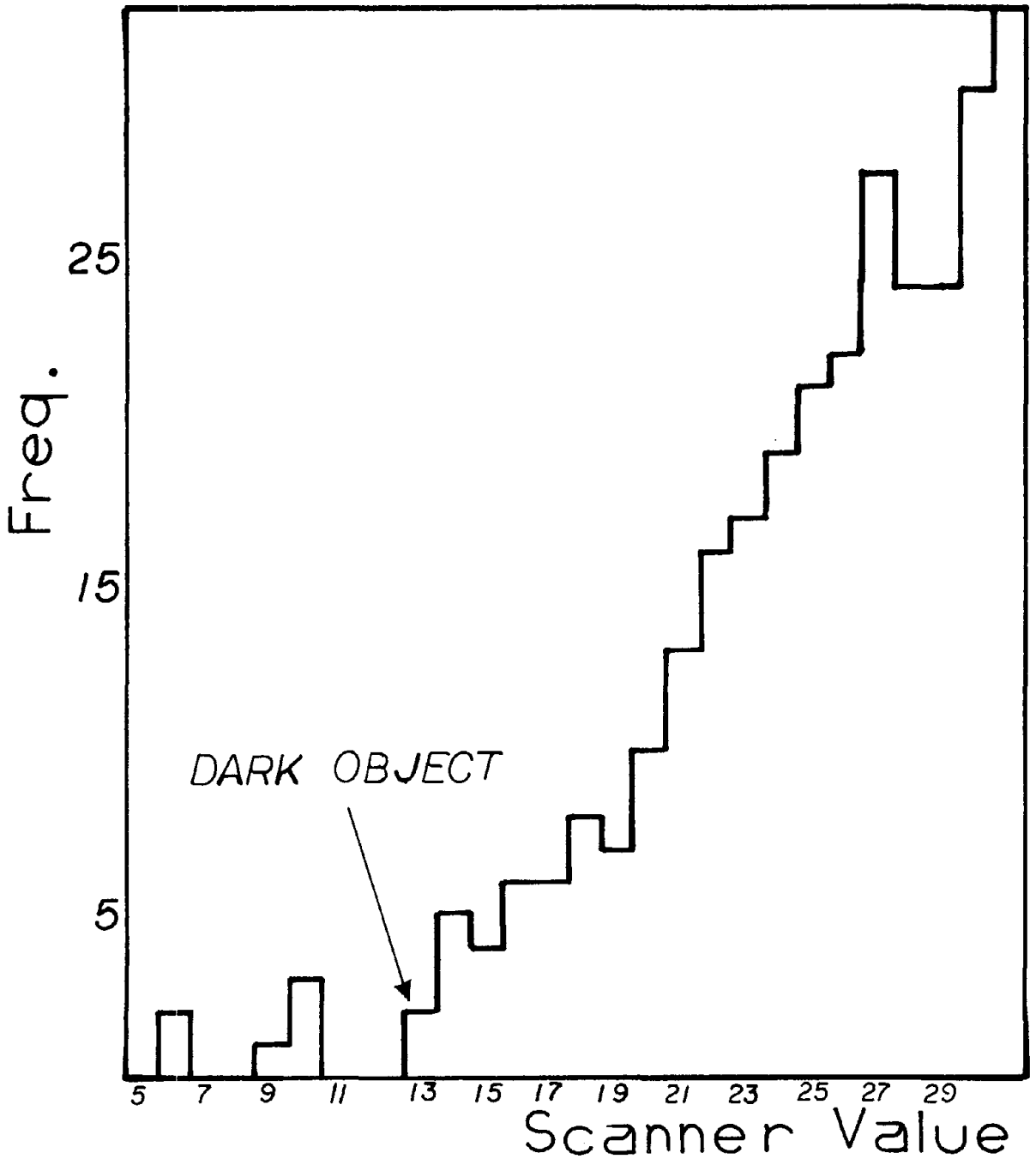

FIGURE 4. HYPOTHETICAL HISTOGRAM OF SCANNER VALUES SHOWING HOW ASC DARK OBJECTS ARE CHOSEN

TABLE 4. COMPARISON OF RECOGNITION USING ASC TRANSFORMED AND UNTRANSFORMED SIGNATURES

Training Data Set	Signature Extension Method	Recognition Data Set	Center-Field Pixel Recognition		
			Correct Wheat		Correct Other
Fay, 11 June	UT	Fay, 10 June	64.0%		89.3%
Fay, 11 June	ASC	Fay, 10 June	89.5%		84.6%
Fay, 11 June	UT	She, 8 June	41.5%		95.9%
Fay, 11 June	ASC	She, 8 June	84.9%		86.3%
			Correct Corn	Correct Soy	Correct Other
White, 21 Aug	UT	Fay, 21 Aug	1.7%	10.0%	70.9%
White, 21 Aug	ASC	Fay, 21 Aug	18.4%	55.9%	92.7%

As can be seen from Table 4 the ASC method, in two of the cases, significantly improved major crop recognition. It should be recalled that the "Correct Other" category includes targets which may not have been recognized as the correct class but which weren't recognized as wheat.

In the next section we will investigate a Type 1 method which does not rely on the assumption of equation (4).

5.2 MASC

MASC is an algorithm which provides a mapping of signatures from one data set to another. It is potentially capable of correcting the differences in signatures caused by variations between the two data sets of:

1. Atmospheric and solar illumination conditions. This includes differences in sun-target-scanner geometries .
2. Electronic gain and other instrumental parameters,
3. And, in an average way, soil type and moisture.

In order to discuss the MASC algorithm we must see how these three sources of variations affect the datum values recorded by the scanner. To do that we will begin with a review of the sources of data variation.

Consider first the radiance received by the scanner from the "mean" of crop α in channel i,

$$L_\alpha^{(i)} = E^{(i)} T^{(i)} \rho_\alpha^{(i)} + L_p^{(i)} \quad ;$$

$E^{(i)}$ is the irradiance incident on the target in channel i, $T^{(i)}$ is the transmittance of the radiation through the atmosphere from the target to the sensor, and $L_p^{(i)}$ is the scattered path radiance in channel i. For two data sets, 1 and 2, a difference in atmospheric and solar illumination conditions will result in different values for $E^{(i)}$, $T^{(i)}$, and $L_p^{(i)}$. Differences in soil

conditions may also result in different values for the reflectance $\rho_\alpha^{(i)}$ for the two data sets. If we further allow for a change in gain, $G^{(i)}$, between the two data sets then the signals actually recorded for the same crop from two different data sets are:

$$S_{\alpha 1}^{(i)} = G_1^{(i)} L_{\alpha 1}^{(i)} = G_1^{(i)} E_1^{(i)} T_1^{(i)} \rho_{\alpha 1}^{(i)} + G_1^{(i)} L_{p1}^{(i)}, \tag{5}$$

$$S_{\alpha 2}^{(i)} = G_2^{(i)} L_{\alpha 2}^{(i)} = G_2^{(i)} E_2^{(i)} T_2^{(i)} \rho_{\alpha 2}^{(i)} + G_2^{(i)} L_{p2}^{(i)}. \tag{6}$$

If we wish to extend the signatures extracted from data set 1 to data set 2, in a way which will yield accurate recognition, then we must find a mapping such that

$$S_{\alpha 2}^{(i)} = A_\alpha^{(i)} S_{\alpha 1}^{(i)} + B_\alpha^{(i)} . \tag{7}$$

By substituting equations (5) and (6) into equation (7) it is found that

$$A_\alpha^{(i)} = \frac{G_2^{(i)} E_2^{(i)} T_2^{(i)} \rho_{\alpha 2}^{(i)}}{G_1^{(i)} E_1^{(i)} T_1^{(i)} \rho_{\alpha 1}^{(i)}} , \tag{8}$$

and

$$B_\alpha^{(i)} = G_2^{(i)} L_{p2}^{(i)} - A_\alpha^{(i)} G_1^{(i)} L_{p1}^{(i)} . \tag{9}$$

Equation (7) defines a multiplicative and additive signature correction (MASC) which maps the signature for crop α in the TDS onto the signature for crop α in the RDS. What is necessary for successful signature extension is to obtain the MASC parameters $A_\alpha^{(i)}$ and $B_\alpha^{(i)}$.

The two parameters $A_\alpha^{(i)}$ and $B_\alpha^{(i)}$ contain the effects of all measurement variables including target reflectance. If the distribution of reflectances for target α is different for the two data sets then the MASC mapping will, in general, not be unique. The two MASC parameters will have an explicit dependence on the target type α. In what follows we will assume that the distributions of reflectances for the various targets are approximately the same for the two data sets. In this way we are able to employ a unique mapping using the parameters $A^{(i)}$ and $B^{(i)}$. If the above assumption does not hold then we will define a unique mapping by the parameters $A^{(i)}$ and $B^{(i)}$ which are the averages over α of the parameters $A_\alpha^{(i)}$ and $B_\alpha^{(i)}$,

$$A^{(i)} \equiv \sum_\alpha a_\alpha^{(i)} A_\alpha^{(i)}$$

$$B^{(i)} \equiv \sum_\alpha b_\alpha^{(i)} B_\alpha^{(i)}$$

where

$$\sum_\alpha a_\alpha^{(i)} = 1$$

$$\sum_\alpha b_\alpha^{(i)} = 1$$

Thus equation (7) becomes

$$S_{\alpha 2}^{(i)} = A^{(i)} S_{\alpha 1}^{(i)} + B^{(i)}. \tag{10}$$

So far everything we have done is formal and of little use unless the MASC parameters can be found for the data sets of interest. If the gain and target reflectances were the same for both data sets, $A^{(i)}$ and $B^{(i)}$ could in theory be obtained by making appropriate atmospheric measurements at the time of data collection. Even this, however, may not be practical for timely large area inventories.

What is required is equivalent "looks" at the two data sets. In this way information concerning the relative natures of the data sets can be obtained without resort to ground observations. One method of obtaining this information quantitatively is with the use of unsupervised clustering. The MASC algorithm which has been developed to obtain $A^{(i)}$ and $B^{(i)}$ uses an ERIM clustering routine [4]. Any good clustering routine should work provided it be applied in exactly the same way to both data sets.

The clustering routine is applied separately to both data sets. (It isn't necessary to cluster over every point in the data set, a sampling, e.g. over every other scan line would be sufficient.) The output from the ERIM clustering routine is a set of clusters. The number of pixels in each cluster is given in the output. The clusters are represented by multivariate Gaussian distributions. Only those clusters are retained which contain more than 1% of all the pixels clustered.

These clusters are unidentified for both data sets; no ground truth has been used. In order to use these clusters to obtain the MASC parameters of equation (10) it is necessary to find a correspondence between the individual clusters of each data set. To form this correspondence we order the clusters of each data set on the basis of their means in one of the channels. Other, perhaps better, methods of forming this correspondence are in the process of being programmed. In the present implementation the channel chosen for this ordering is the channel with the largest range of values. After both sets of clusters have been ordered in this way a one to one correspondence is made -- the number one cluster of data set one is

[4] H. M. Horwitz, J. T. Lewis and A. P. Pentland, "Estimating Proportions of Objects From Multispectral Scanner Data", ERIM Report No. 109600-13-F, April 1975, Section 4.4 and Appendix E.

matched up with the number one cluster of data set two, etc. Using the means of the Gaussian distributions representing the clusters as points defining a line

$$C_2^{(i)} = \hat{A}^{(i)} C_1^{(i)} + \hat{B}^{(i)} ,$$

where the $C_2^{(i)}$ and $C_1^{(i)}$ are the set of cluster means in channel i for data set 2 and data set 1 respectively; a regression routine is used to determine the parameters $\hat{A}^{(i)}$ and $\hat{B}^{(i)}$. These parameters are then applied to the signatures of the TDS, as in equation (10), and the resulting transformed signatures can be applied to the RDS.

The basic assumption behind this MASC algorithm is that the two data sets contain the same types of targets, although not necessarily in the same proportions. If the correspondence of unidentified clusters in the manner described is to have any validity this assumption must hold at least approximately. Forming such correspondences would make little sense if one data set was agricultural and the other was woodlands, or urban.

The test of any signature extension method lies in its performance on real data. The results of applying MASC to our data sets are listed in Table 5 which gives the data set from which the signatures were derived and the data set to which they were extended. The results are for field-center-pixel recognition.* Also listed are the results of applying untransformed (UT) signatures.

We see that the MASC algorithm results in significant improvement in major crop recognition for all three cases. Also there is very little change in "Correct Other".

Both Type 1 methods we have investigated have been found to be potentially viable signature extension methods for large area crop surveys.

*The multiplicative terms, $A^{(i)}$, were used to scale the signature covariances as well as the signature means.

TABLE 5. RECOGNITION USING UNTRANSFORMED AND MASC SIGNATURES

Training Data Set	Signature Transformation Applied	Recognition Data Set	Center-Field-Pixel Recognition	
			Correct Wheat	Correct Other
Fay, 11 June	UT	Fay, 10 June	64.0%	89.3%
Fay, 11 June	MASC	Fay, 10 June	93.0%	84.2%
Fay, 11 June	UT	She, 8 June	41.5%	95.9%
Fay, 11 June	MASC	She, 8 June	83.0%	95.0%

Training Data Set	Signature Transformation Applied	Recognition Data Set	Center-Field-Pixel Recognition		
			Correct Corn	Correct Soy	Correct Other
White, 21 Aug	UT	Fay, 21 Aug	1.7%	10.0%	70.9%
White, 21 Aug	MASC	Fay, 21 Aug	83.4%	83.2%	72.2%

6
TYPE 2 SIGNATURE EXTENSION METHODS

As described in section 1, a Type 2 method is one which requires the preprocessing of both the TDS and RDS. This preprocessing is performed in an attempt to remove the effects of variations in the relative measurement conditions of the two data sets. In this section we investigate two Type 2 methods: Ratios of Spectral Bands, and RADIFF. While both methods had worked well with aircraft data in the past they failed to perform satisfactorily, in terms of recognition, on LANDSAT-1 data. The reasons for these failures are discussed.

6.1 RATIOS OF SPECTRAL BANDS

Ratios of Spectral Bands (Ratios) [5,6] is a Type 2 signature extension technique. It requires the preprocessing of every data point in both the training and recognition data sets.

The preprocessing of the data consists of forming new channels which are the ratio of the scanner signals in two of the LANDSAT-1 bands. Because there are four MSS LANDSAT-1 bands one can form three independent ratio channels. As we will see, the usefulness of the Ratio method depends on two assumptions concerning the relative measurement conditions between the TDS and RDS:

1) The variations in target reflectance, between the TDS and RDS, are systematic in the sense that a variation in one channel is matched by variations in the other channels.

2) There is no path radiance term in the signals of either data set.

A further restriction on the usefulness of the Ratio method is imposed by the fact that the separation between the target signatures is reduced when

---

[5] R. K. Vincent, G. S. Thomas and R. F. Nalepka, "Signature Extension Studies", ERIM Report No. 190100-26-T, July 1974.

[6] R. F. Nalepka and J. P. Morgenstern, "Signature Extension: An Approach to Operational Multispectral Surveys", ERIM Report No. 31650-152-T, March 1973.

the Ratio channels are formed. This may not be true for other data sets where interclass variation is large.

As seen previously, the signal for target α in channel i is given by

$$S_\alpha^{(i)} = G^{(i)}[\rho_\alpha^{(i)} E^{(i)} T^{(i)} + L_p^{(i)}],$$

where $G^{(i)}$ is the system gain in channel i, $E^{(i)}$ is the total downward irradiance incident on the target, $T^{(i)}$ is the transmittance which effectively attenuates the reflected radiation from the target, $\rho_\alpha^{(i)}$ is the reflectance of the target, and $L_p^{(i)}$ is the path radiance which has been scattered into the field of view from something other than the target. A ratio channel is formed from the signals in two of the MSS channels:

$$R_\alpha^{(ij)} = \frac{S_\alpha^{(i)}}{S_\alpha^{(j)}}$$

$$= \frac{G^{(i)}}{G^{(j)}} \quad \frac{\rho_\alpha^{(i)} E^{(i)} T^{(i)} + L_p^{(i)}}{\rho_\alpha^{(j)} E^{(j)} T^{(j)} + L_p^{(j)}} \quad .$$

If we denote the TDS with the subscript 1 and the RDS with the subscript 2 then for the two data sets we have:

$$R_{\alpha 1}^{(ij)} = \frac{\rho_{\alpha 1}^{(i)} G_1^{(i)} E_1^{(i)} T_1^{(i)} + L_{p1}^{(i)} G_1^{(i)}}{\rho_{\alpha 1}^{(j)} G_1^{(j)} E_1^{(j)} T_1^{(j)} + L_{p1}^{(j)} G_1^{(j)}}$$

and

$$R_{\alpha 2}^{(ij)} = \frac{\rho_{\alpha 2}^{(i)} G_2^{(i)} E_2^{(i)} T_2^{(i)} + L_{p2}^{(i)} G_2^{(i)}}{\rho_{\alpha 2}^{(j)} G_2^{(j)} E_2^{(j)} T_2^{(j)} + L_{p2}^{(j)} G_2^{(j)}} \quad .$$

We now assume that the variation in the terms $G^{(i)}E^{(i)}T^{(i)}$ is matched by a similar variation in $G^{(j)}E^{(j)}T^{(j)}$, i.e.,

$$G_2^{(i)}E_2^{(i)}T_2^{(i)} = (1 + \delta)G_1^{(i)}E_1^{(i)}T_1^{(i)}$$

and

$$G_2^{(j)}E_2^{(j)}T_2^{(j)} = (1 + \delta)G_1^{(j)}E_1^{(j)}T_1^{(j)} \quad .$$

Using this variation we can write

$$R_{\alpha 2}^{(ij)} = \frac{\rho_{\alpha 2}^{(i)}G_1^{(i)}E_1^{(i)}T_1^{(i)}(1+\delta) + L_{p2}^{(i)}}{\rho_{\alpha 2}^{(j)}G_1^{(j)}E_1^{(j)}T_1^{(j)}(1+\delta) + L_{p2}^{(j)}} \quad .$$

Now making our two assumptions, namely:

1) $$\frac{\rho_{\alpha 2}^{(i)}}{\rho_{\alpha 2}^{(j)}} = \frac{\rho_{\alpha 1}^{(i)}}{\rho_{\alpha 1}^{(j)}} \quad ,$$

2) $$L_{p2}^{(i)} = L_{p2}^{(j)} = L_{p1}^{(i)} = L_{p1}^{(j)} = 0$$

we find that

$$R_{\alpha 2}^{(ij)} = \frac{\rho_{\alpha 1}^{(i)}G_1^{(i)}E_1^{(i)}T_1^{(i)}}{\rho_{\alpha 1}^{(j)}G_1^{(j)}E_1^{(j)}T_1^{(j)}} = R_{\alpha 1}^{(ij)} \quad .$$

Thus the Ratio channels, if the above assumptions hold, will yield "universal" signatures in the sense that the crop signatures will be the same for both data sets 1 and 2.

If the assumptions of the Ratio method hold approximately then the method could prove useful for extending signatures. However, due to the spectral characteristics of the LANDSAT-1 scanner the RATIO method has not proven to be too successful with present satellite data. The LANDSAT-1 bands are very broad and widely separated therefore the condition that any change in $G^{(i)}E^{(i)}T^{(i)}$ is matched by a similar variation in $G^{(j)}E^{(j)}T^{(j)}$ is probably not well satisfied. Also the shapes of the spectral curves for the various vegetative types are very similar in the LANDSAT channels. Most of the discriminatory information is contained in the relative magnitudes of the signals. When Ratio channels are formed a good deal of the magnitude information is lost, while differences in spectral shape are emphasized. To see this quantitatively we look at the separation between signals for the various vegetative crops. For the four LANDSAT channels typical values for the separation are

$$\frac{S_\alpha^{(i)} - S_\beta^{(i)}}{1/2(S_\alpha^{(i)} + S_\beta^{(i)})} \approx 10\text{-}20\%,$$

where S_α and S_β are the signature means of wheat and grass for F6-11. For the Ratio channels, however, the separation is much smaller:

$$\Delta_{\alpha\beta}^{(ij)} = \frac{R_\alpha^{(ij)} - R_\beta^{(ij)}}{1/2(R_\alpha^{(ij)} + R_\beta^{(ij)})} \approx 1\text{-}3\%.$$

Thus the ability to discriminate between crops α and β is reduced when Ratio channels are used. It should be noted that the Ratio technique has been found to be quite effective when other scanners, e.g. aircraft, are used.

If one is to attempt to employ ratios for identifying different vegetative types then the channels to be ratioed must be chosen so that $\Delta_{\alpha\beta}^{(ij)}$ is maximized. A more rigorous method of choosing the channels is to compute the pairwise probability of misclassification, PPM, for all possible ratios and then choose

the best set of three ratios. Using this method for the F6-10 data set one obtains the ratio set 2/4, 3/1, 3/4. Using the first criterion the best set obtained is 2/4, 3/1, 3/2. A comparison of the results using these two ratio sets on the test fields of F6-10 using the F6-10 signatures is shown in Table 6.

TABLE 6. COMPARISON OF PPM AND MAX $\sum_{\alpha,\beta} w_{\alpha\beta}\Delta_{\alpha\beta}^{(ij)}$ CRITERION

Ratio Set	% Recognition of Wheat	% Correct Other
(2/4, 3/1, 3/4)	52.6%	93.0%
(2/4, 3/1, 3/2)	55.3%	95.7%

Thus the use of the criterion that a weighted sum $\sum_{\alpha,\beta} w_{\alpha\beta}\Delta_{\alpha\beta}^{(ij)}$, be maximized, ($w_{\alpha\beta}$ represents a weighting of the vegetative types to be distinguished), while not rigorously justified, seems to be a useful method for choosing ratio channels.

Using this ratio set to extend the F6-11 signatures to F6-10, (see Table 7), does not improve recognition results. It should be noted however that an optimum set of Ratios for one data set may be sub-optimum for a different data set.

TABLE 7. RECOGNITION OF F6-10 TRAINING AND TEST FIELDS

Signatures	% Recognition of Wheat	% Correct Other
F6-11 UT	64.0%	89.3%
F6-11 (2/4,3/1,3/2)	64.0%	88.2%

6.2 RADIFF*

RADIFF (ratio of differences) [7] is a Type II signature extension method. It provides a means of preprocessing the data such that, if certain assumptions hold, the three types of variation listed in the MASC section are eliminated from the data.

From the results of calculating the path radiance using the ERIM Radiative Transfer Model it was found that the ratio of path radiance in adjacent channels was approximately constant. In order to take advantage of this fact the RADIFF method has been developed.

We shall begin by deriving the equations that define the RADIFF transformation and then will point out the assumptions which are implicit in those equations. Starting with equation (1) for the signal recorded in channel i for a particular crop type, α, in data set 1:

$$S_{\alpha 1}^{(i)} = G_1^{(i)} E_1^{(i)} T_1^{(i)} \rho_{\alpha 1}^{(i)} + G_1^{(i)} L_{p1}^{(i)} , \tag{11}$$

where again $G_1^{(i)}$, $E_1^{(i)}$, $T_1^{(i)}$, and $L_{p1}^{(i)}$ are, respectively, the gain, total downward irradiance, transmittance and path radiance for data set 1 in channel i and $\rho_{\alpha 1}^{(i)}$ is the reflectance of crop α in channel i for data set 1. We now form a new channel:

$$S_{\alpha 1}^{(i,i+1,i+2)} \equiv \frac{S_{\alpha 1}^{(i)} - S_{\alpha 1}^{(i+1)} K_{i,i+1}^{1}}{S_{\alpha 1}^{(i+2)} - S_{\alpha 1}^{(i+1)} K_{i+2,i+1}^{1}} , \tag{12}$$

where

$$K_{i,i+1}^{1} \equiv \frac{L_{p1}^{(i)}}{L_{p1}^{(i+1)}} .$$

---

*The general concept for RADIFF was developed under the name DIFF/DIFF. See reference [7].

[7] R. F. Nalepka and J. P. Morgenstern, "Signature Extension: An Approach to Operational Multispectral Surveys", ERIM Report No. 31650-152-T, March 1973, p. 36.

Using equation (11) in equation (12) we find that

$$S_{\alpha 1}^{(i,i+1,i+2)} = \frac{C_{i,i+1}^{1} \frac{\rho_{\alpha 1}^{(i)}}{\rho_{\alpha 1}^{(i+1)}} - K_{i,i+1}^{1}}{C_{i+2,i+1}^{1} \frac{\rho_{\alpha 1}^{(i+2)}}{\rho_{\alpha 1}^{(i+1)}} - K_{i+2,i+1}^{1}} , \tag{13}$$

where

$$C_{i,i+1}^{1} \equiv \frac{G_1^{(i)} E_1^{(i)} T_1^{(i)}}{G_1^{(i+1)} E_1^{(i+1)} T_1^{(i+1)}} .$$

In deriving equation (13) we have assumed that the gain factor is the same for each channel, i.e.,

$$G_1^{(i)} = G_1^{(i+1)} = G_1^{(i+2)} \quad \text{etc.}$$

We now make the additional assumptions that,

1) Any variation in the path radiance in one channel is matched in the adjacent channel. Thus: we assume that the ratio

$$K_{i,i+1}^{1} = \frac{L_{p1}^{(i)}}{L_{p1}^{(i+1)}}$$

is independent of the particular atmospheric state, i.e., the ratio of path radiances can be written as $K_{i,i+1}$.

2) In the same way any variation in the product $E^{(i)}T^{(i)}$ is matched in the adjacent channel, thus the factor $C_{i,i+1}^{1}$ becomes $C_{i,i+1}$ and is independent of atmospheric state.

If these assumptions hold then the new RADIFF channel will be independent of atmospheric state. If we further assume that we are interested in extending signatures to data sets for which the crop reflectances do not vary, then the RADIFF channel should have the same value for each crop in all data sets:

$$S_{\alpha 1}^{(i,i+1,i+2)} = S_{\alpha 2}^{(i,i+1,i+2)} = \ldots = S_{\alpha n}^{(i,i+1,i+2)} = S_{\alpha}^{(i,i+1,i+2)}$$

If all of the above assumptions hold then the RADIFF transformation will yield universal crop signatures. The degree to which the universality of the RADIFF signatures fails is a reflection of the limited degree to which the assumptions are satisfied. In order to form the RADIFF channels (equation (12)) we must calculate the values for the $K_{i,i+1}$, at the same time we can test the assumption that they are independent of atmospheric state. The independence of the $C_{i,i+1}$ could be examined in the same way but this has not as yet been done. For purposes of using the RADIFF channels we wish in particular to form $S^{(1,2,3)}$ and $S^{(2,3,4)}$. We thus must calculate $K_{1,2}$, $K_{3,4}$, and $K_{2,3}$. The ERIM Radiative Transfer model was used to calculate the path radiance for a number of atmospheric states, as described by visibility values (see Fig. 5). These values for L_p were then integrated over simulated LANDSAT bands as shown in Fig. 6. The results of the integration are given in Table 8. Finally the ratios $K_{1,2}$, $K_{2,3}$, and $K_{3,4}$ were formed and are plotted versus visibility in Fig. 7. Also shown in Fig. 7 are the averages of the ratios over visibility and the maximum variation from this average. As can be seen, the assumption that the K's are constant over atmospheric state is correct within approximately 10%.

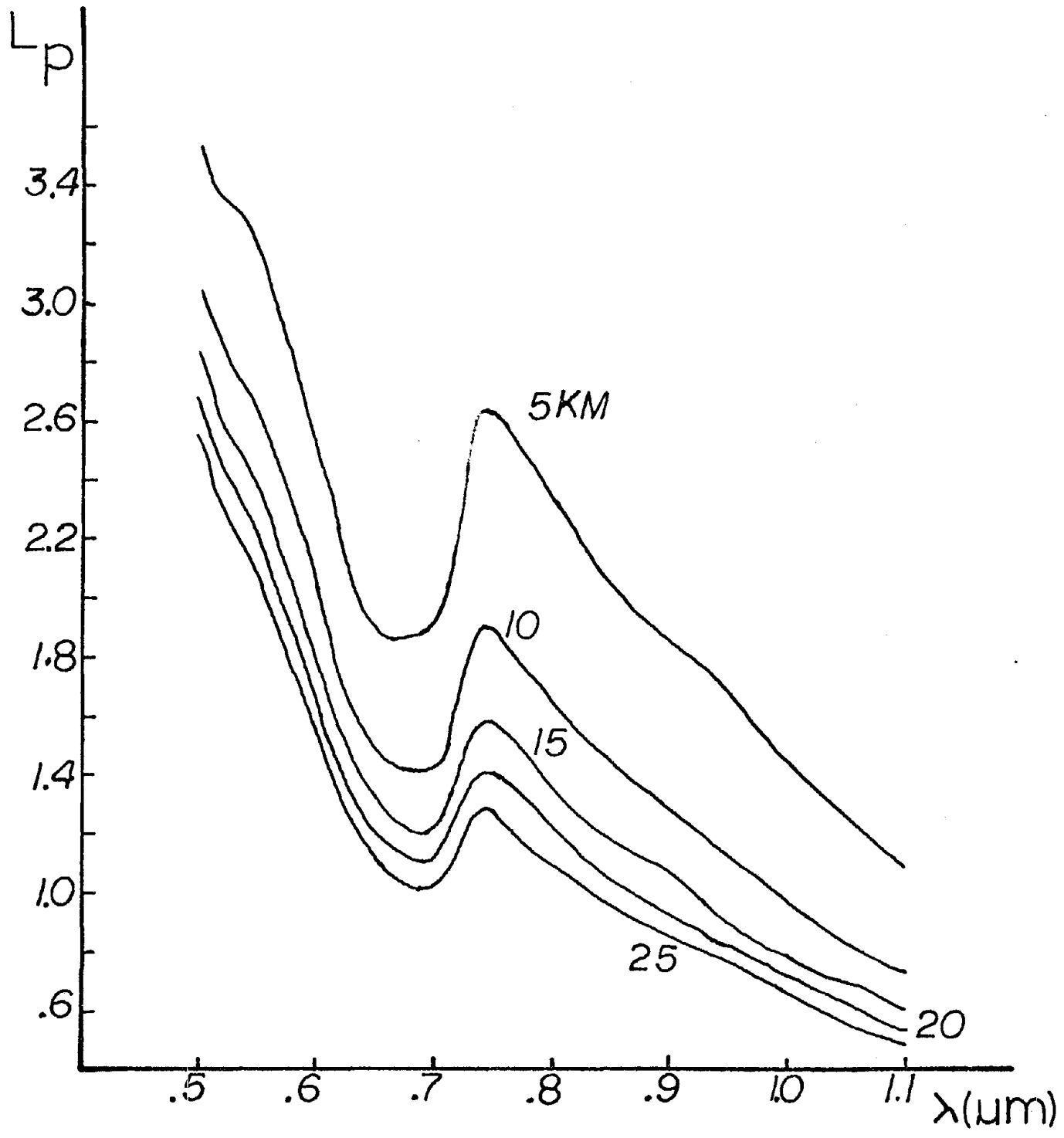

FIGURE 5. PATH RADIANCE (m watts/cm^2/steradian/μm) VS. WAVELENGTH. Alt. = 910 km, Solar Zenith = 62°, Green Vegetation Target on Green Vegetation Background. (Calculation based on ERIM Radiative Transfer Model). Visibility = 5 km, 10 km, 15 km, 20 km, 25 km.

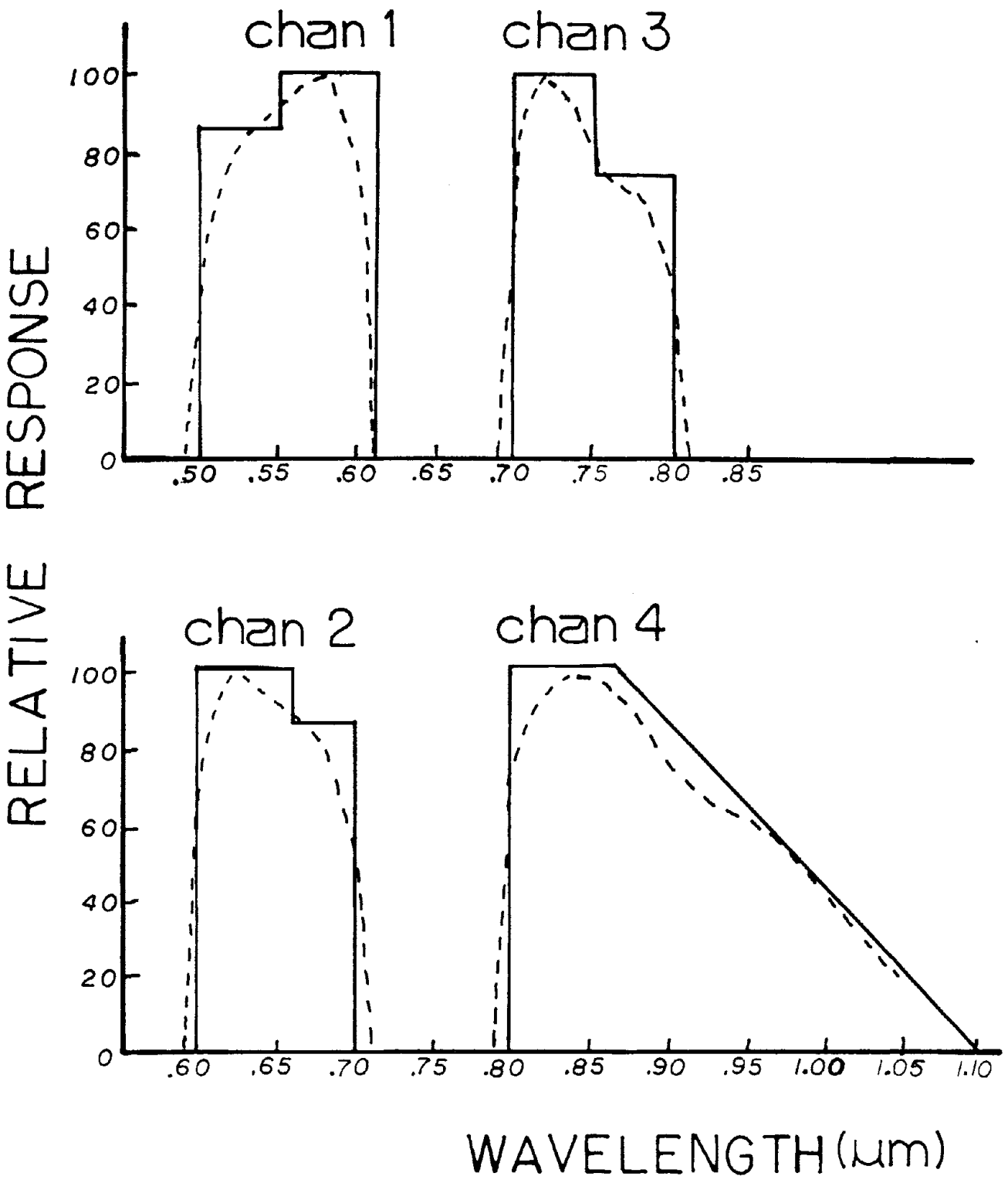

FIGURE 6. RELATIVE RESPONSE OF LANDSAT-1 VS. WAVELENGTH.
Actual LANDSAT-1 - - - - -
Simulation for Integration ————

TABLE 8. PATH RADIANCE INTEGRATED OVER LANDSAT-1 BANDS

Channel / Visibility	1	2	3	4
5 km	2.79	2.06	2.33	1.86
10 km	2.45	1.60	1.70	1.32
15 km	2.22	1.40	1.42	1.09
20 km	2.07	1.28	1.27	.98
25 km	1.95	1.19	1.16	.88

The channels $S^{(2,3,4)}$ and $-[S^{(1,2,3)}]^{-1}$ were formed for both the F6-11 and F6-10 data sets. (Note: the latter channel was formed in that particular way to insure that it was positive and greater than 1.0.) The values used for the K's were the average values as shown in Fig. 7. Training was then accomplished using the training fields of F6-11 and these signatures were then used to perform recognition on the F6-10 data set. The results are listed in Table 9.

TABLE 9. RECOGNITION OF F6-10 USING F6-11 RADIFF SIGNATURES

Center Field Pixel Recognition	
Correct Wheat	Correct Other
64.0%	85.4%

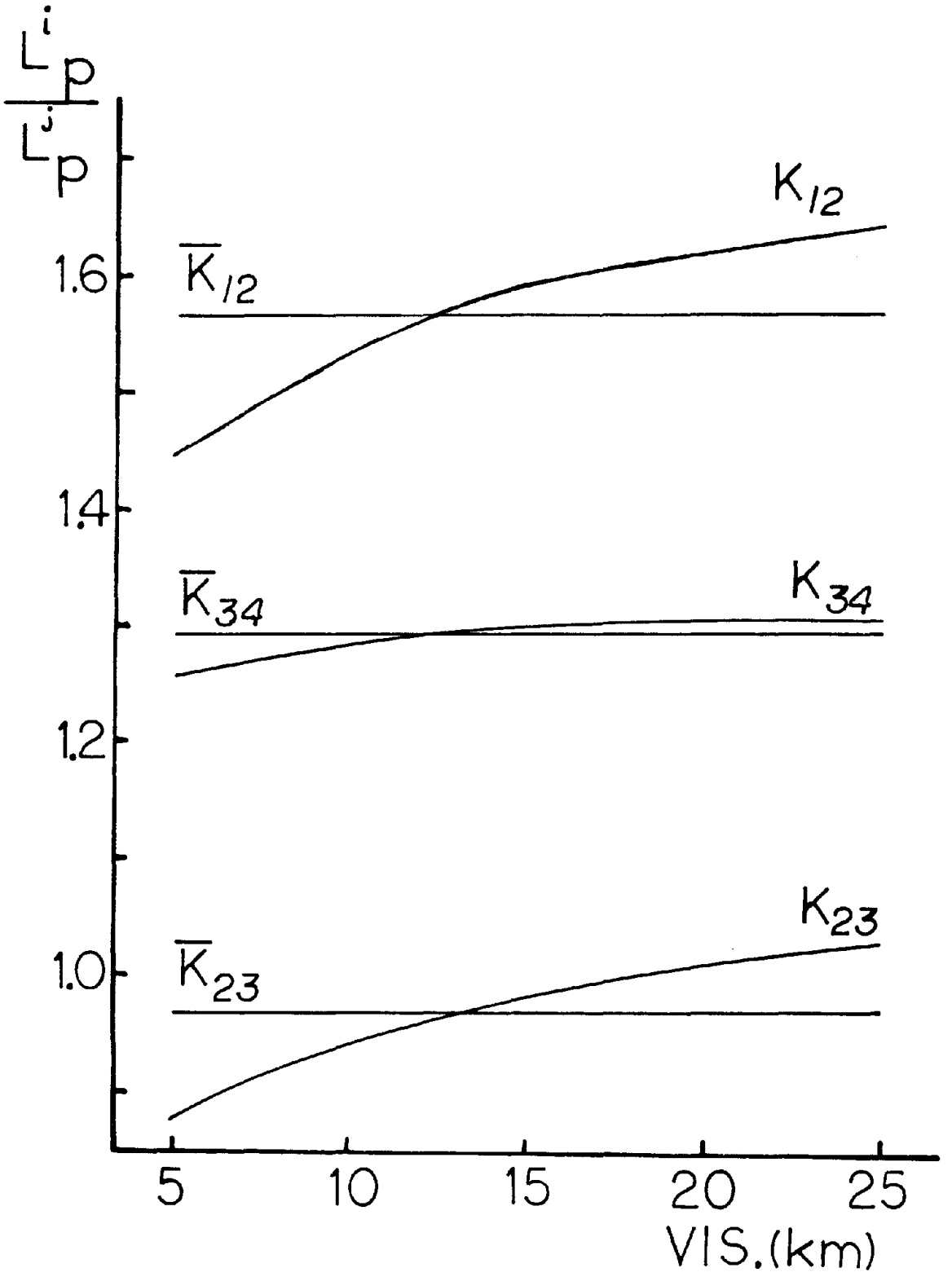

FIGURE 7. RATIO OF PATH RADIANCE VS. VISIBILITY.
$\overline{K}_{12} = 1.5668$, $\overline{K}_{23} = .9676$, $\overline{K}_{34} = 1.2922$

These results are not as good as the MASC or ASC results. At this point it is not possible to say if the poor results are due to the failure of the basic assumptions to not be satisfied exactly. It may be necessary to recalculate the K's with better approximations to the response functions of the LANDSAT-1 scanner. It may also be necessary to restrict the limits of applicability of the model so that the assumptions are more nearly obtained. It is also possible that in forming the RADIFF channels, i.e., preprocessing the data, the information content of the signals may be reduced. This in turn could be either due to round-off errors in the calculation of the RADIFF channels or it may be inherent in the nature of the transform. Further investigations are required to answer these questions.

7

EXPERIMENT TO DETERMINE EFFECT OF ATMOSPHERIC-GEOMETRIC VARIATIONS ON RECOGNITION

As discussed in a previous section, there are a number of variables which could lead to changes in the target signatures when going from one data set to another. One of the possible sources of variation results from a change in sensor gain. Since this is strictly an instrumental variation, and our experiment will involve two data sets taken only one day apart, we will assume that the gain is a constant. It is, of course, difficult to determine if, in fact, this is the case, but, in light of the calibration methods [8], it seems to be a good assumption.

For the purpose of this experiment the other sources of variation can be considered to fall into two classes. The first class is essentially composed of on the ground variations. These include changes in soil type, and moisture content, cultural practices (irrigation and fertilization), and changes in crop maturity. The second class consists of variations in sun angle (time of day), atmospheric profile (optical depth, aerosol content, etc.), and scanner view angle. The question which this experiment attempts to answer is: what is the effect on recognition of variations in only atmospheric profile and scanner view angle? This question is of importance because the current LACIE approach may not adequately correct for these variables. These two variables will result in both additive and multiplicative changes while the MLA (mean level adjustment) yields only an additive correction.

In order to answer the question we have posed it is necessary to find two data sets for which, to the best of our knowledge, the only variables are atmosphere and scanner view angle. Fortunately in the CITARS study two such data sets were available. These were the Fayette June 10 and June 11

[8] ERTS Data Users Handbook, NASA Document No. 71SD4249, Appendix G.

data sets (F6-10 and F6-11). In particular we will consider only the training fields which were identified in the CITARS study. Thus we have two data sets composed of exactly the same fields; the only difference between the two sets is that they were collected on successive days. Obviously, since we are looking at the same fields only one day apart (there was no rainfall between the collection of the data sets), factors such as soil type, and moisture content can be assumed constant. Further, since both data sets were collected at the same time of day the sun angle is not a variable.

To see that the state of maturity of the wheat was constant we plot mean signature values obtained from both F6-10 and F6-11 in Fig. 8. The upper line for each target is the mean signature value from F6-10 and the lower lines are the mean signature values from F6-11. As can be seen there is no substantial change in the wheat signature going from F6-10 to F6-11 which is not reflected in the change in the signature for trees. The weed signature shows a similar variation. For the June period, a change in maturity for wheat would primarily be due to "browning", i.e., loss of chlorophyll. This would in turn result in an increase in reflectance in channel 2. In fact, however, the signature for wheat in channel 2 for F6-11 is lower than for F6-10. We can therefore assume from this analysis that the state of maturity of wheat is not a variable when going from F6-11 to F6-10.

Thus the primary variables are atmosphere and scanner view angle. While on the ground horizontal visibility readings were the same for both June 10 and June 11 at nearby airports, there was one obvious difference in the atmospheres for June 10 and June 11 in the imagery of the respective LANDSAT frames. While the June 10 frame was clear of all clouds there were some small cumulus clouds in the June 11 frame. Neither these clouds, nor their shadows, covered any of the training fields.

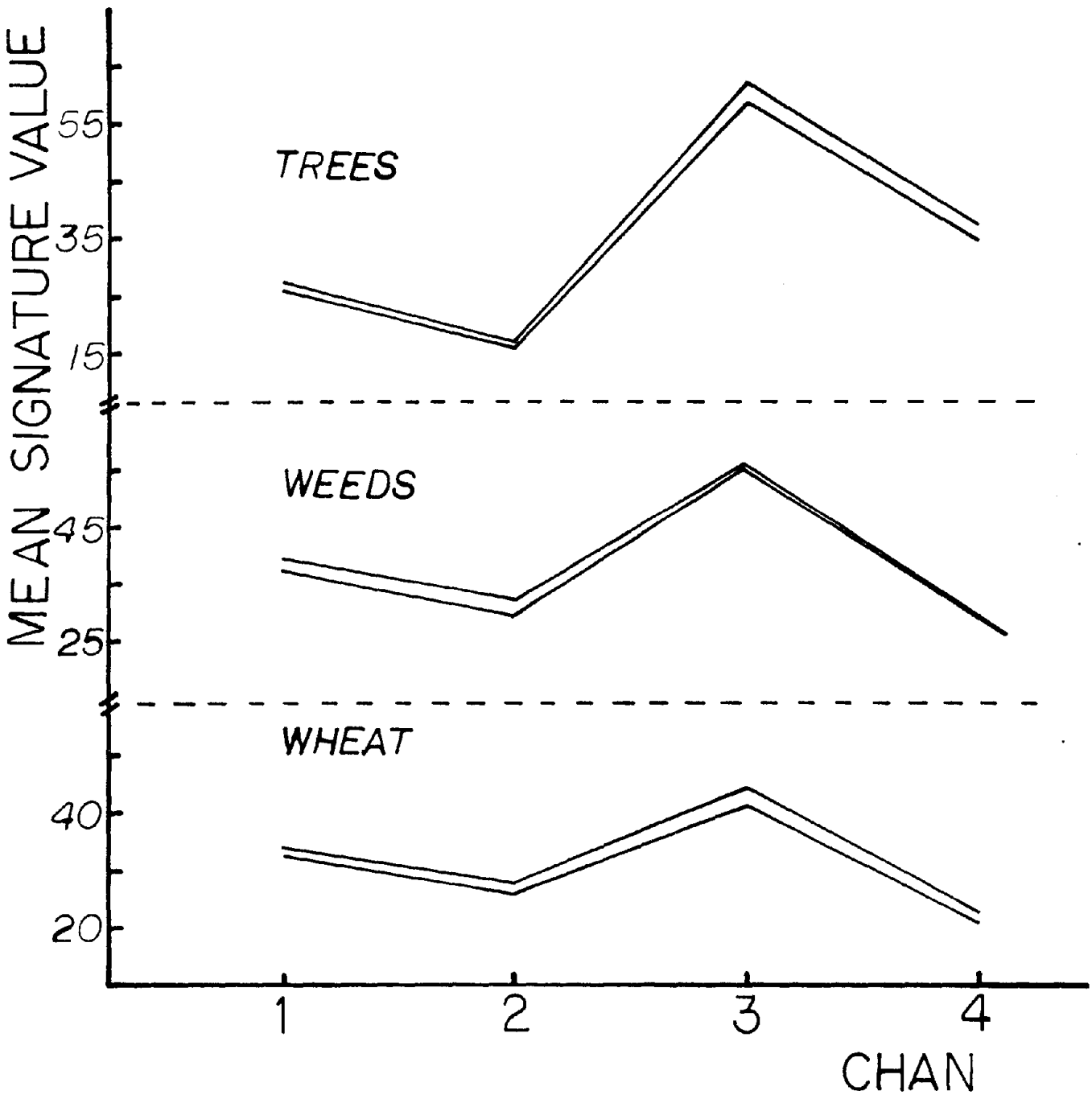

FIGURE 8. COMPARISON OF MEAN SIGNATURE VALUES FOR FAY 6-10 AND FAY 6-11. Upper curve for each crop is mean signature value for F6-10; lower curves are for F6-11.

Because the data were collected 24 hours apart there was a small difference in scanner view angle (see Fig. 9). For the data taken on the 10^{th} the view angle was approximately $2^{\circ}50'$ west of nadir while on the 11^{th} it was approximately $3^{\circ}40'$ east of nadir. Thus there was more than a 6° difference in view angle.

In order to test the effect of variations in atmosphere and scanner view angle on recognition we derive our training statistics from all of the training fields from F6-11. These signatures are then used for recognition on the very same fields for both F6-11 and F6-10. Obviously if the variations in atmosphere and view angle do not affect recognition accuracy then the results should be approximately the same for both F6-11 and F6-10. As can be seen in Table 10 there is a clear reduction in recognition accuracy when signatures from F6-11 are applied to F6-10.

TABLE 10. RECOGNITION RESULTS OF FAY 6-11 AND FAY 6-10 TRAINING FIELDS USING F6-11 SIGNATURES

Recognition Data Set	Central Field Recognition	
	Correct Wheat	Correct Other
Fay 6-11, Training	91.6%	97.2%
Fay 6-10, Training	72.9%	97.7%

We see, therefore, that variations in atmosphere and scanner view angle alone can seriously affect recognition. As discussed in the previous section the MASC algorithm has the capability of correcting for these variations, as well as other possible variations. In Table 11 we give the results of applying the MASC algorithm to the F6-11 signatures and then using them to perform recognition on the F6-10 training fields.

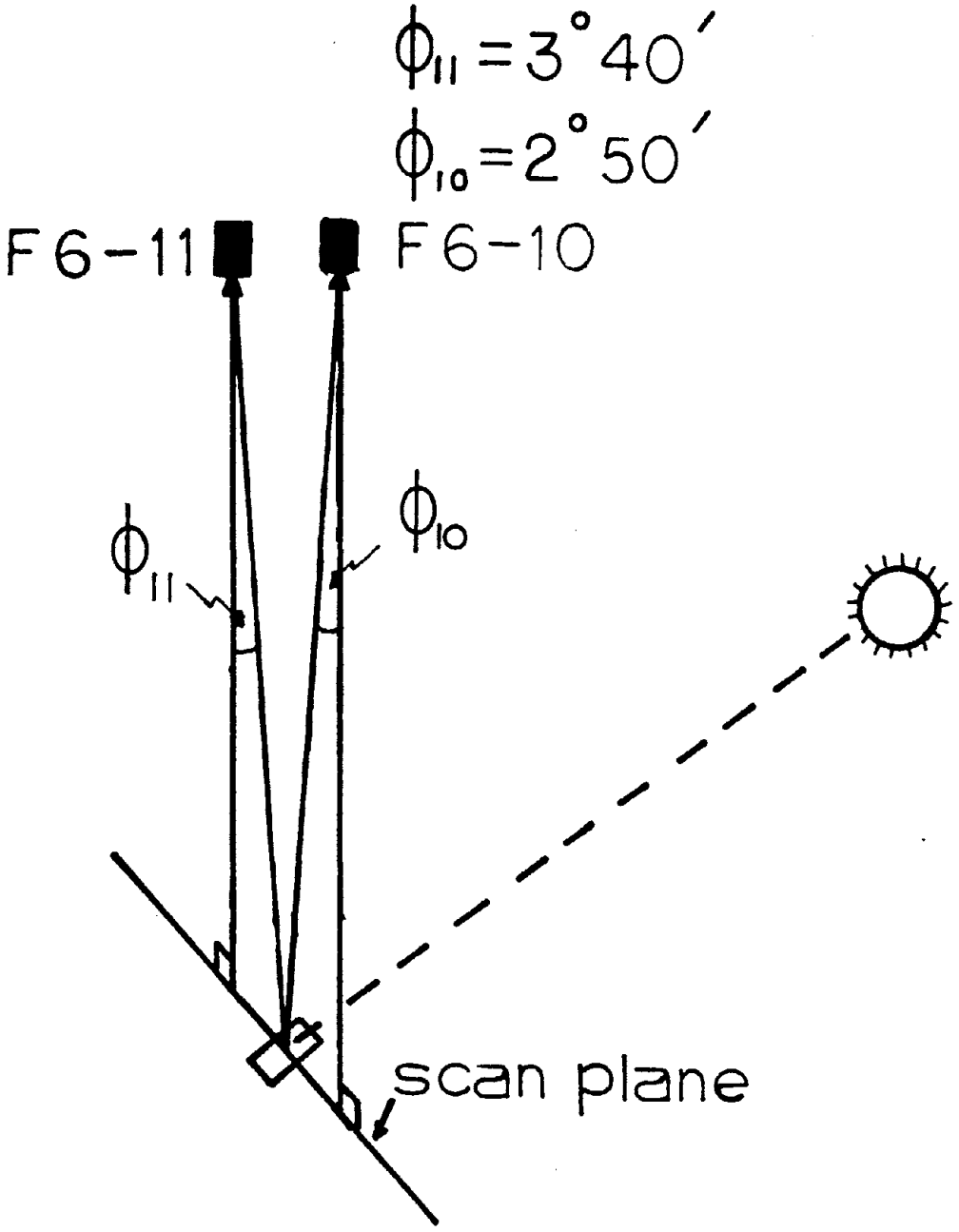

FIGURE 9. RELATIVE GEOMETRY OF DATA COLLECTION FOR FAYETTE, JUNE 10 (F6-10) AND FAYETTE, JUNE 11 (F6-11).

TABLE 11. RECOGNITION OF F6-10 TRAINING FIELDS USING MASC TRANSFORMED SIGNATURES FROM F6-11

Data Set	Central Field Recognition	
	Correct Wheat	Correct Other
F 6-10 Training	100%	94.3%

Because of the nature of the data collection it is difficult to separate the effects of atmospheric state and scanner view angle. This experiment clearly demonstrates, however, that one or both of these effects can have a real impact when recognition with extended signatures is attempted. In the future we hope to be able to separate these effects by using atmospheric and canopy models in conjunction with real data and the MASC algorithm. It should be noted that the results of the CITARS study have demonstrated that there is a direct correlation between the degradation of non-local recognition (using untransformed signatures) and the difference in optical depth between the TDS and RDS [9].

[9] Personal communication from R. M. Bizzell.

8

DETERMINING TRAINING FIELDS WITHOUT IN SITU GROUND INFORMATION

Signature extension is one approach to reducing the large amounts of ground information required for operational crop surveys. Another approach which may prove fruitful is to attempt to determine training sites, for each data set, without the use of in situ ground information. In this section we will describe some initial attempts to attack the problem in this way.

Our approach is based on the assumption that regions of multi-dimensional MSS data space can be defined such that each region contains the MSS data for a single spectral vegetation class. In addition it is assumed that each region is uniquely defined for all data sets in terms of its relationship to every other region of the space. If these assumptions are to hold then it is necessary that the same crops exist in both data sets. The maturity of the various crops should be approximately the same for both data sets.

Rather than examine the entire LANDSAT-1 four-dimensional data space we will deal only with the sub-space of channels 2 and 3. This reduction of the space causes only a slight loss of information since there is a high degree of correlation between channels 1 and 2 and between channels 3 and 4 (see Figures 10 and 11). In order to visualize the pattern formed by the data in our subspace we cluster over the data set and plot two-dimensional (channels 2 and 3) representations of the clusters. Each cluster is represented by a one standard deviation ellipse. The cluster mean is located within each ellipse by a point. The clusters are labeled, for identification purposes, by the first two digits (see Figure 12). The second two digits represent the percentage of all the points clustered over which are included in the cluster. Percentages less than 1% are represented

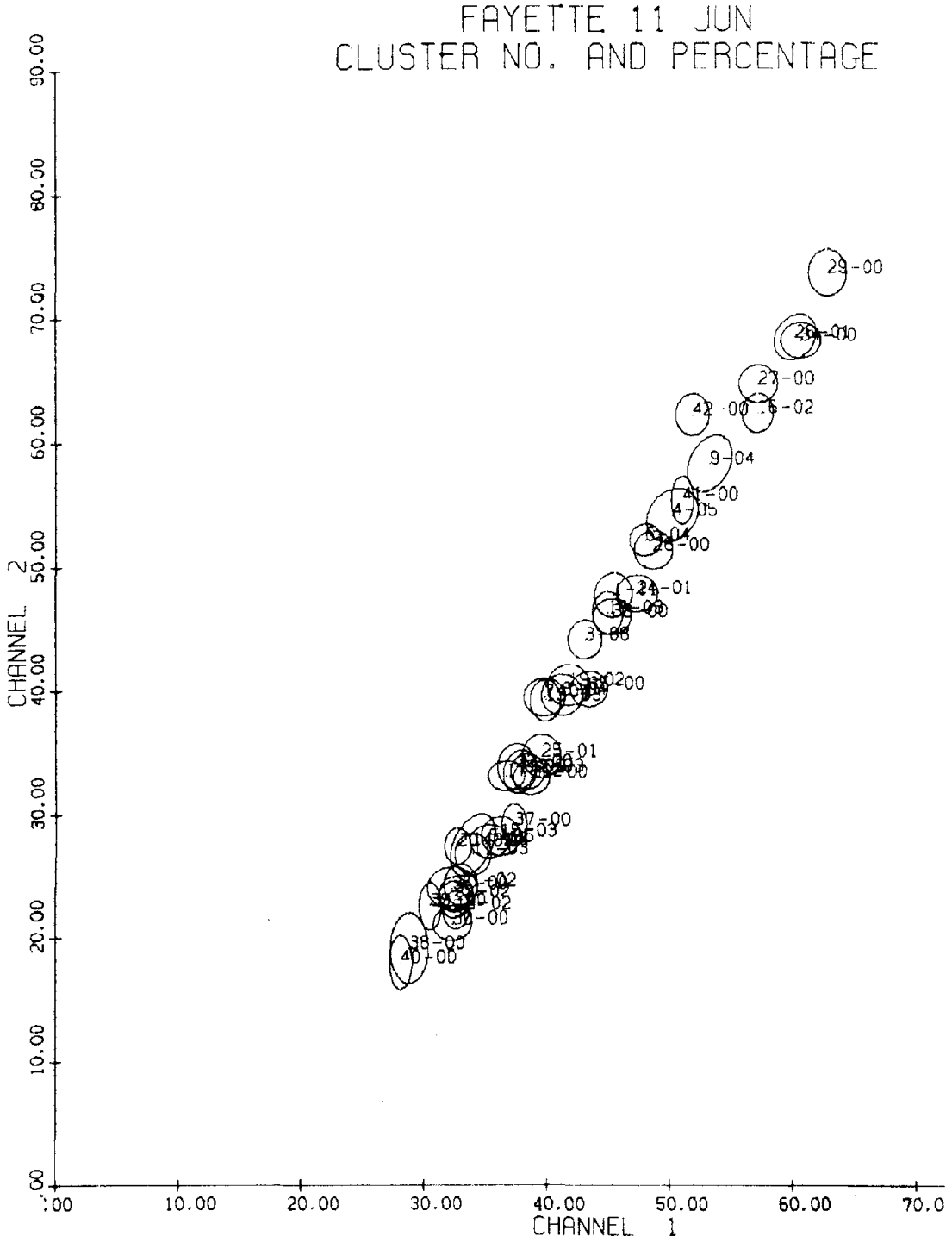

FIGURE 10. CLUSTER PLOT OF F6-11 SHOWING HIGH CORRELATION BETWEEN CHANNELS 1 AND 2

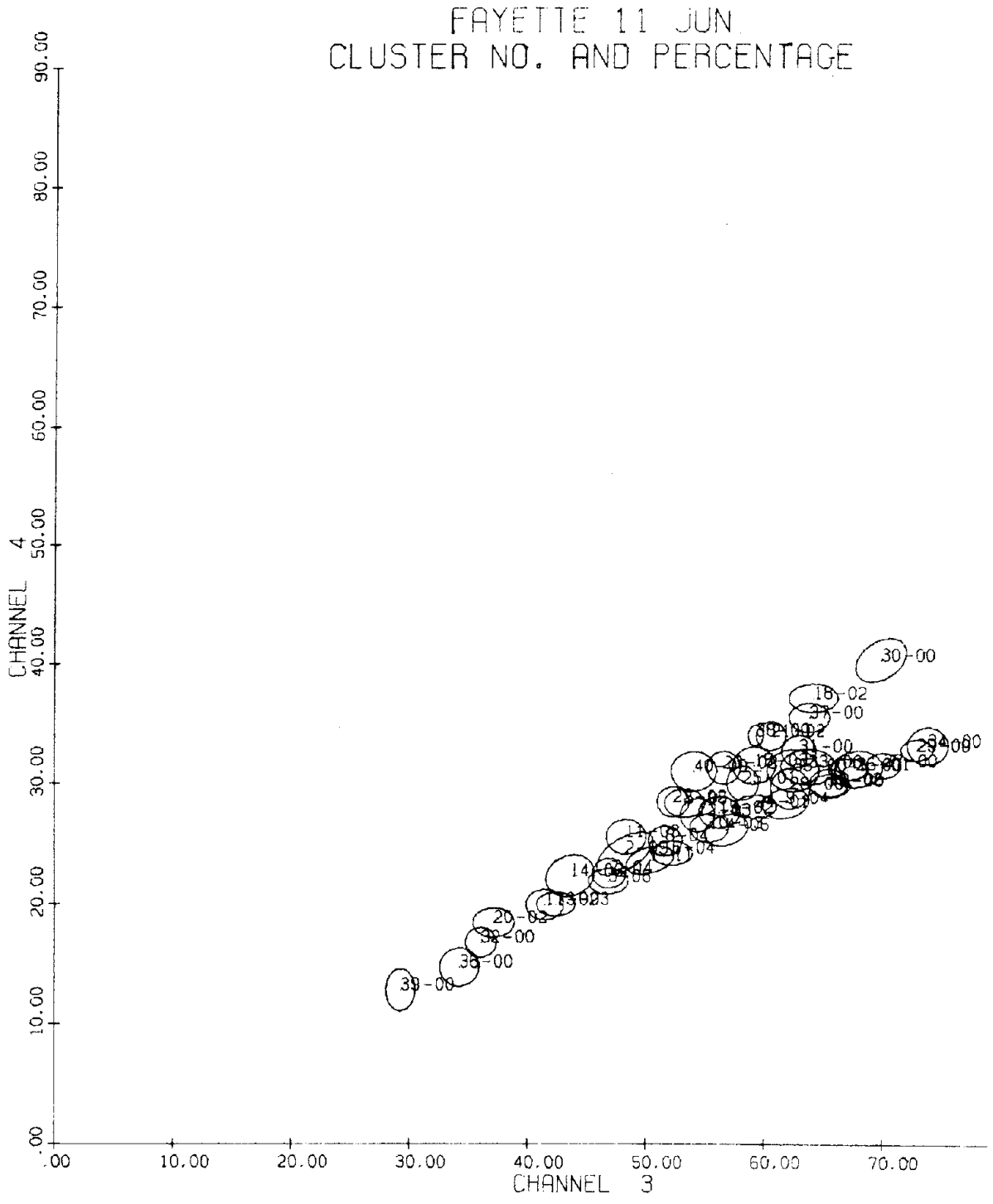

FIGURE 11. CLUSTER PLOT OF F6-11 SHOWING HIGH CORRELATION BETWEEN CHANNELS 3 AND 4

by double zeros while all other percentages are rounded off to the nearest integer percentage.

For purposes of displaying the general pattern, clustering was performed over the quarter sections which contained the training fields identified by the CITARS project. This subset of the entire data set was chosen to save computation time. A better method may be to sample over the entire data set.

The resulting cluster plots for F6-11 and S6-8 are shown in Figures 12 and 13. Refering to Figure 12 we see that the general pattern is triangular. The vertices of the triangle being clusters 39, 29 and 30. This form turns out to be quite general for agricultural data sets. The side of the triangle extending from 39 to 29 represents a progression of bare soil types from darker to lighter soils. The sides from 29 to 30 and 39 to 30 represent variations in such scene parameters as percent vegetation cover, plant geometry, leaf structure, etc. coupled with the soil effects. For a more detailed interpretation of the general cluster pattern, see Appendix III. If we could identify a region of this triangular pattern as belonging to a particular crop type then by mapping the triangle from F6-11 into the triangular pattern for S6-8 we would obtain a mapping of the single crop region from F6-11 to S6-8. The clusters which fall within this crop region of S6-8 could then be used to identify fields for training on that crop. The clusters within the crop region of S6-8 may also be used to perform recognition on S6-8.

Two methods were used to map the triangular pattern from F6-11 into the triangular pattern of S6-8. These were the Overlay Method and the Method of Affine Transformations (MAT). In addition to these two methods the MASC algorithm may prove useful in the future. The MASC algorithm is a restricted type of affine transformation.

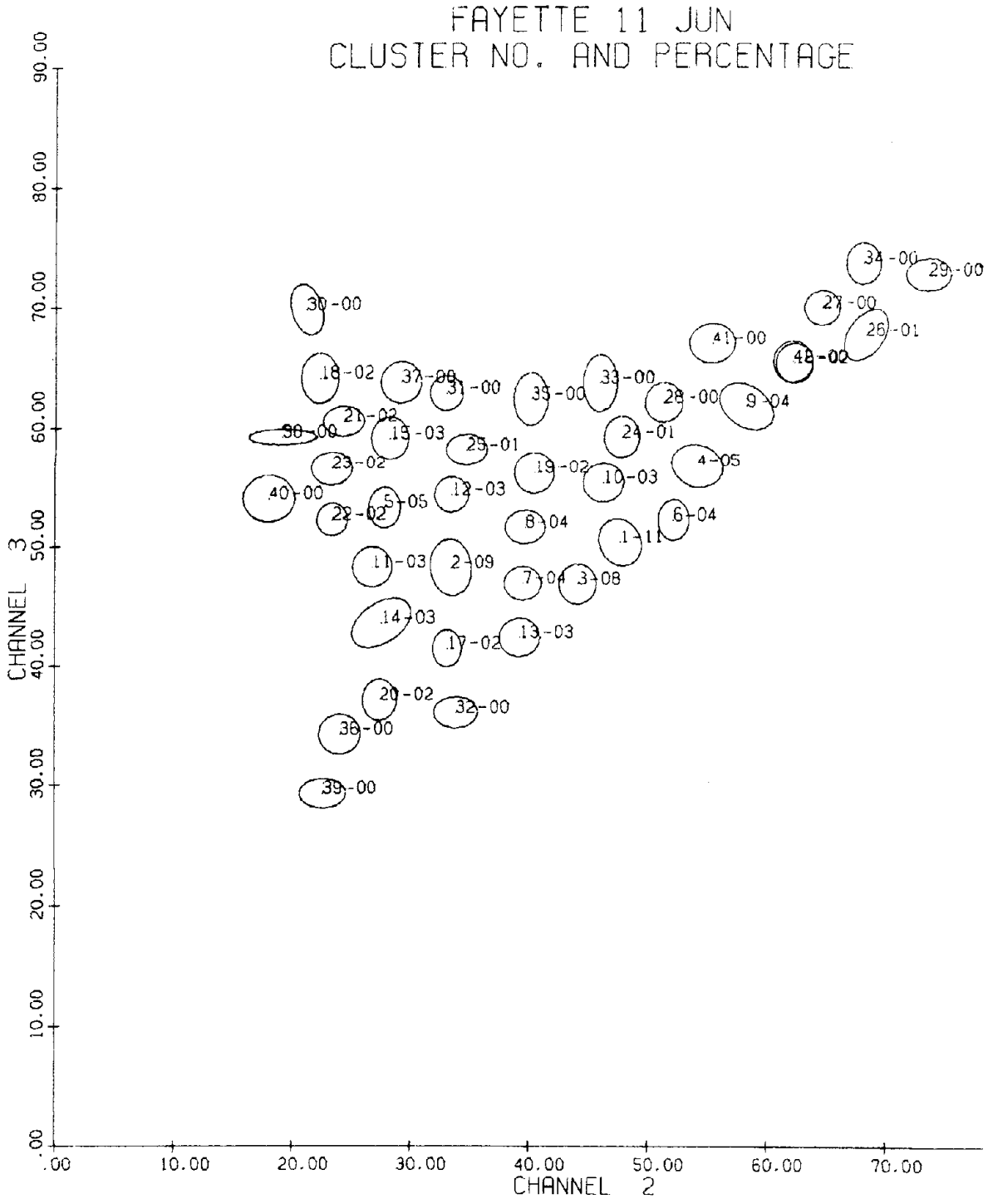

FIGURE 12. GENERAL CLUSTER PATTERN OF F6-11 IN CHANNELS 3 AND 2

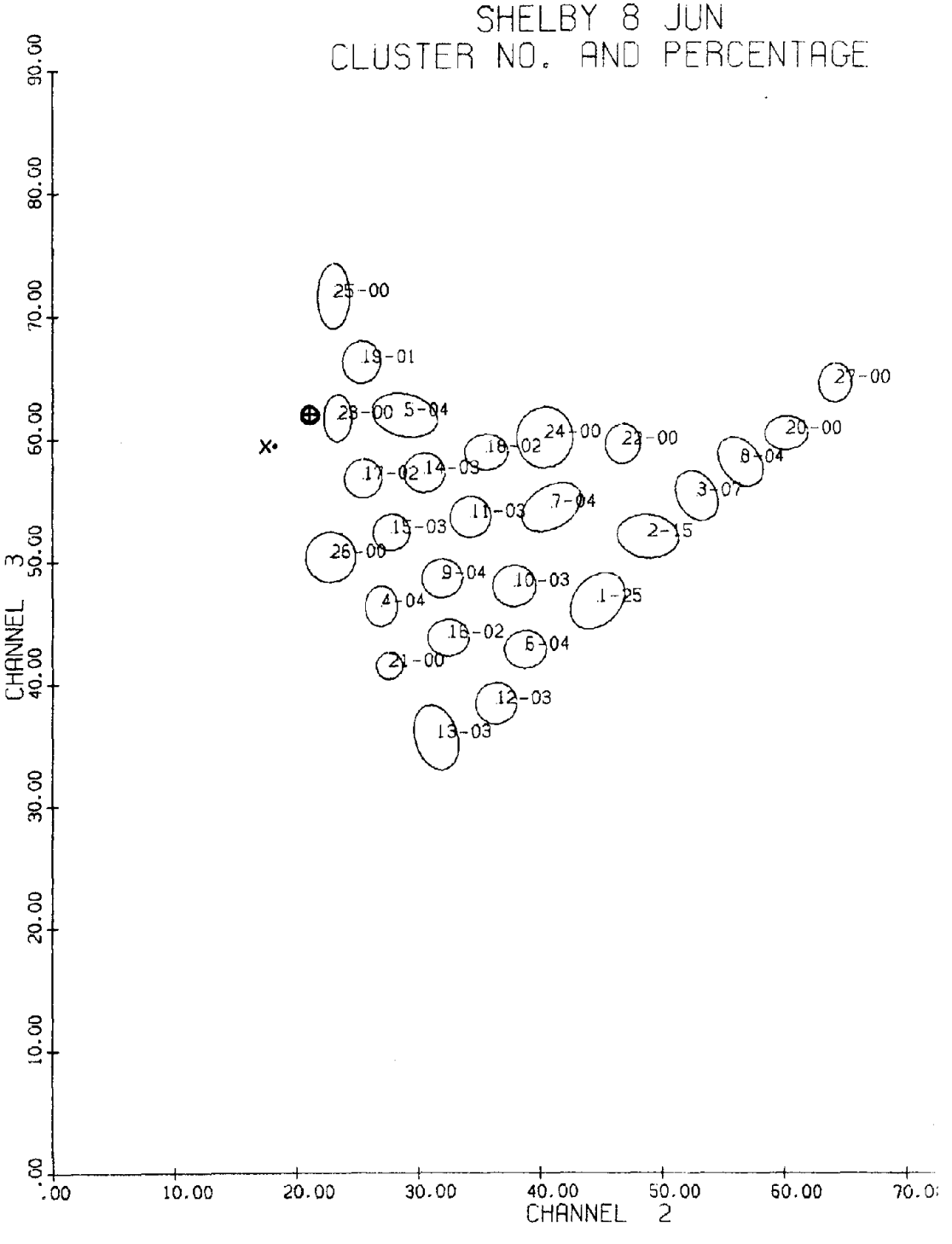

FIGURE 13. GENERAL CLUSTER PATTERN FOR S6-8 IN CHANNELS 3 AND 2. The dot represents the location of the S6-8 tree cluster. X and ⊕ are the positions of the tree cluster transferred from F6-11 by the Overlay and MAT methods, respectively.

The Overlay Method consists of physically overlaying the cluster plot of F6-11 on top of the cluster plot of S6-8. The F6-11 plot is then adjusted, by translations and rotations, until a "best fit" of the two triangular patterns is obtained. This of course involves the judgement of the analyst.

The Method of Affine Transformations consists of choosing the means of the three vertex clusters of the two triangular patterns to define a general affine transformation. Thus the cluster means of clusters 39, 29 and 30 define three points in the F6-11 space while clusters 13, 27 and 25 are used to define the equivalent points in the S6-8 space. These two sets of points are then used to derive a transformation matrix which allows a mapping from F6-11 to S6-8 as described below.

The affine transformation can be written as

$$[M] = \underset{\sim}{A}[N] \ , \tag{14}$$

where $\underset{\sim}{A}$ is the matrix which transforms the space N into the space M. For our purposes the space N corresponds to F6-11 while M corresponds to S6-8. Since we are working with two dimensions we will define our spaces by two vectors $\vec{m}_1, \vec{m}_2$ and $\vec{n}_1, \vec{n}_2$. We define these vectors as:

$$\begin{aligned} \vec{m}_1 &= \text{Cluster 29 - Cluster 39} \\ \vec{m}_2 &= \text{Cluster 30 - Cluster 39} \end{aligned} \tag{15}$$

and

$$\begin{aligned} \vec{n}_1 &= \text{Cluster 27 - Cluster 13} \\ \vec{n}_2 &= \text{Cluster 25 - Cluster 13} \end{aligned} \tag{16}$$

What we have done in equations (15) and (16) is translate the origin in the F6-11 plot to cluster 39 and the origin in S6-8 to cluster 13. In this way we are building into the transformation matrix, $\underset{\sim}{A}$, a translation. We have reduced the spaces M and N to two x two matrices so that equation (14) becomes

$$\underset{\sim}{M} = \underset{\sim}{A}\,\underset{\sim}{N}$$

which can easily be solved for $\underset{\sim}{A}$, formally,

$$\underset{\sim}{A} = \underset{\sim}{M}\,\underset{\sim}{N}^{-1} \quad .$$

The transformation matrix for going from F6-11 to S6-8, derived in the above manner is

$$\underset{\sim}{A} = \begin{bmatrix} .801 & -.178 \\ -.208 & .880 \end{bmatrix} \quad .$$

The diagonal elements of $\underset{\sim}{A}$ correspond to the multiplicative constants of the MASC algorithm. In fact the MASC multiplicative constants can be written in matrix form (for the transformation from F6-11 → S6-8) as

$$\underset{\sim}{A}_{MASC} = \begin{bmatrix} .902 & 0 \\ 0 & .652 \end{bmatrix} \quad .$$

The fundamental difference between a linear transformation of the MASC type and a general affine transformation is the exclusion of rotations of the axis. This rotation is represented by the non-zero off-diagonal matrix elements. In the case of MSS data, where the axis are spectral channels, the non-zero off-diagonal elements can be interpreted as resulting from some dissimilarity

between the two data sets. This dissimilarity may be due to some different crop types or to different reflectances for some of the crop types. Another possibility is that the use of only three points to define the transformation is not precise enough so that the off-diagonal elements are "accidently" non-zero.

In order to test the effectiveness of the two methods they will be used to locate the position of trees in the S6-8 pattern space. This object class was chosen because there were relatively few clusters representing it and because trees were known to be rather distinct, spectrally, from most other object classes. This pattern may be observed by comparing Figure 14 with Figure 12 and Figure 15 with Figure 13. Three clusters were obtained for trees for F6-11 and one cluster for S6-8. Of the F6-11 clusters, cluster 1 contains the majority of the pixels. The two methods will be tested by how close they are able to map the tree cluster 1 from F6-11 onto the tree cluster of S6-8. This mapping is shown on Figure 13 where the "X" locates the mapping as obtained using the Overlay Method. The mapping using the MAT is located by the "$\oplus$". The actual position of the S6-8 tree cluster is located by the dot. As can be seen from Figure 13, the Overlay Method came closer to mapping the F6-11 tree cluster onto the S6-8 tree cluster. It should also be noted, however, that the tree cluster of S6-8 does not fall within the pattern formed by clustering over the quarter sections. This seems to support the idea of increasing the size of the data sample operated on by the clustering algorithm. A larger sample size would increase the probability of including the wide range of soils and soil covers probable in any data set.

The actual mapping of crop regions and the use of those crop regions to define clusters which can be used to identify training fields has not, as yet, been attempted. In the future, the further development of these methods may prove valuable for the location of training fields without in situ ground information.

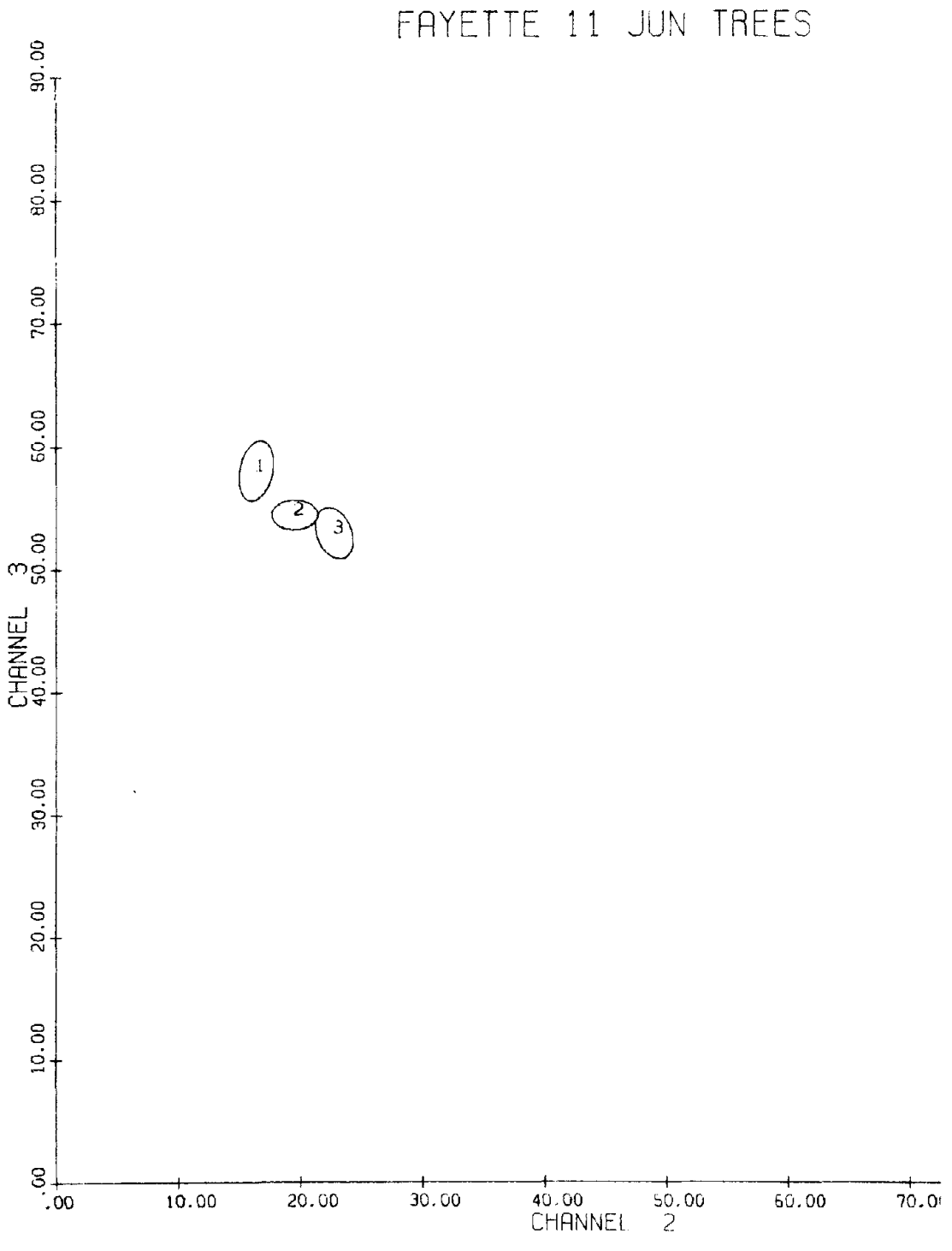

FIGURE 14. TREE CLUSTERS FROM THE TEST FIELDS OF F6-11

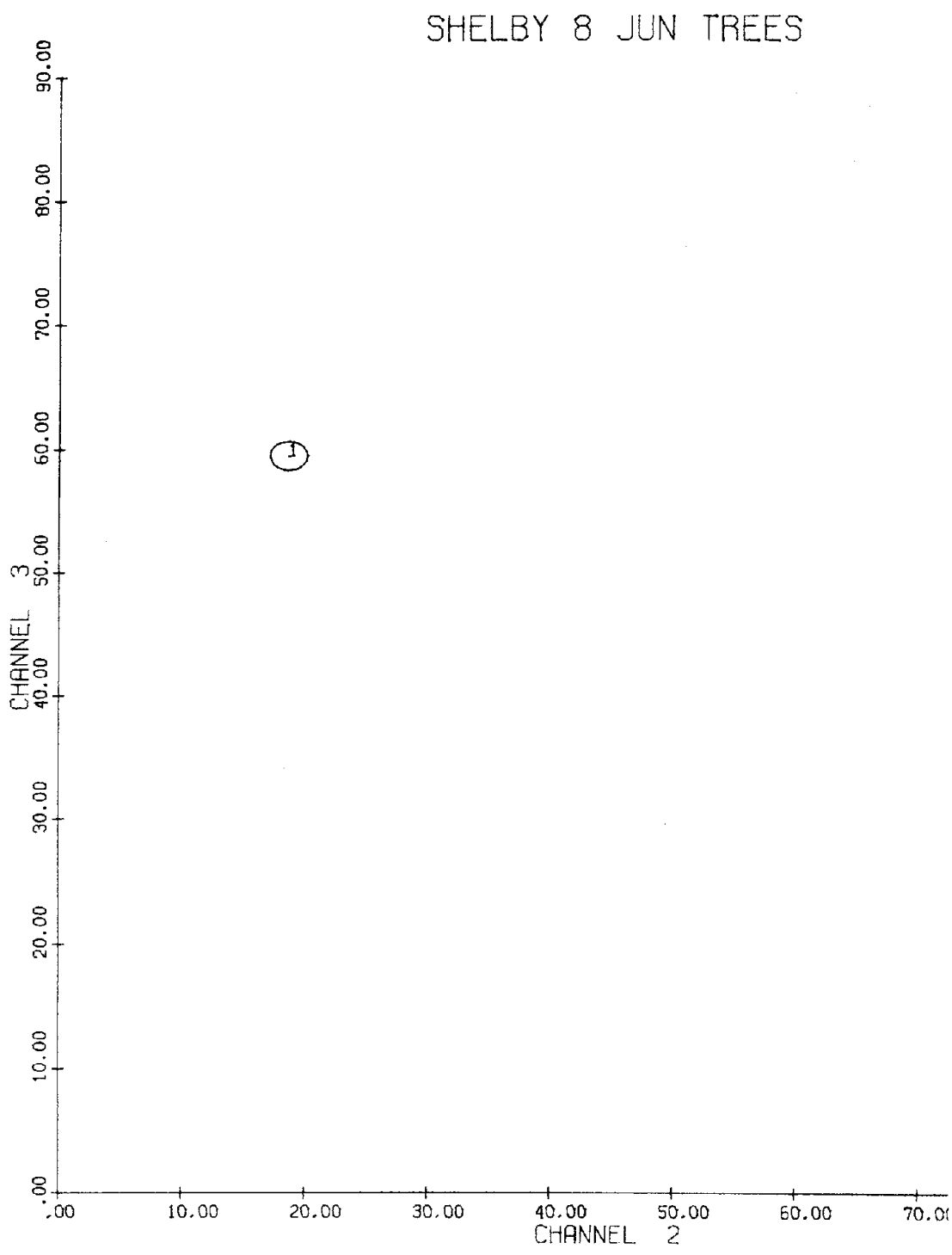

FIGURE 15. TREE CLUSTER FROM THE TEST FIELDS OF S6-8

CONCLUSIONS AND RECOMMENDATIONS

We have shown that the use of untransformed signatures from a TDS, when applied to a temporally-spatially removed RDS, yield poor recognition results. We have investigated the sources of data variability which are responsible for the degraded recognition results. From this investigation four signature extension methods have suggested themselves.

In Fig. 16 we display the F6-10 recognition results using untransformed (UT) F6-11 signatures as well as F6-11 signatures modified by our four methods: Ratio, RADIFF, ASC and MASC. In Fig. 17 and Fig. 18 we display the recognition results using UT, MASC and ASC signatures from F6-11 on S6-8 and from W8-21 on F8-21. We see that the ASC and MASC methods are quite successful -- the MASC method showing significant improvement in recognition in all three cases. In addition, if we plot the average probabilities of misclassification, Fig. 19, we see that the MASC algorithm is fairly constant in its performance. The UT signatures result in more variation in performance. Since the variations between respective TDS and RDS are random, the relative constancy of the average probability of misclassification implies that the MASC algorithm is indeed capable of correcting for those variations.

The MASC algorithm, in particular, may prove helpful in further isolating the physical factors which are the cause of the variations in data between the TDS and RDS. For instance the ERIM Radiative Transfer model can be used to calculate the multiplicative and additive constants based on equations (8) and (9) with the added assumptions that the atmospheric state is the only variable. In Figures 20 and 21 we have plotted the multiplicative and additive constants based on such a calculation and as were derived using the MASC algorithm. While the values can not be expected to match exactly the curves should have similar shapes if we have not neglected an important source of variation. As seen in Figures 20 and 21 the shapes of the MASC curves and the model curves are quite similar. The one exception is between channels one and two for the multiplicative constant. The additive constant depends both on a correct calculation of the path radiance and of the multiplicative constant. The large differences in

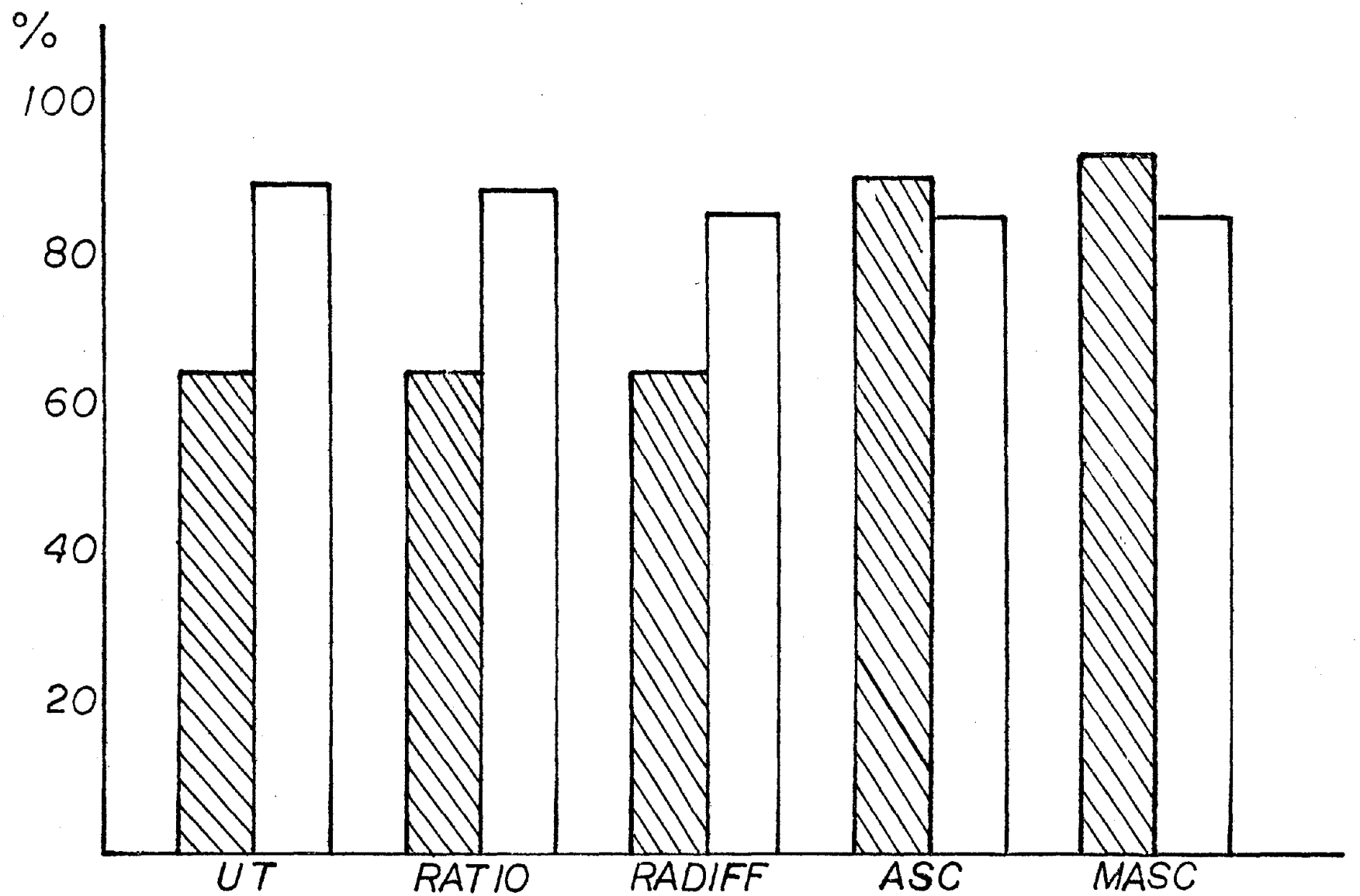

FIGURE 16. RESULTS OF RECOGNITION EXPERIMENT ON F6-10 USING VARIOUS TRANSFORMATIONS ON THE F6-11 SIGNATURES. The striped bar is the percentage correct wheat recognition. The open bar is percentage other correct.

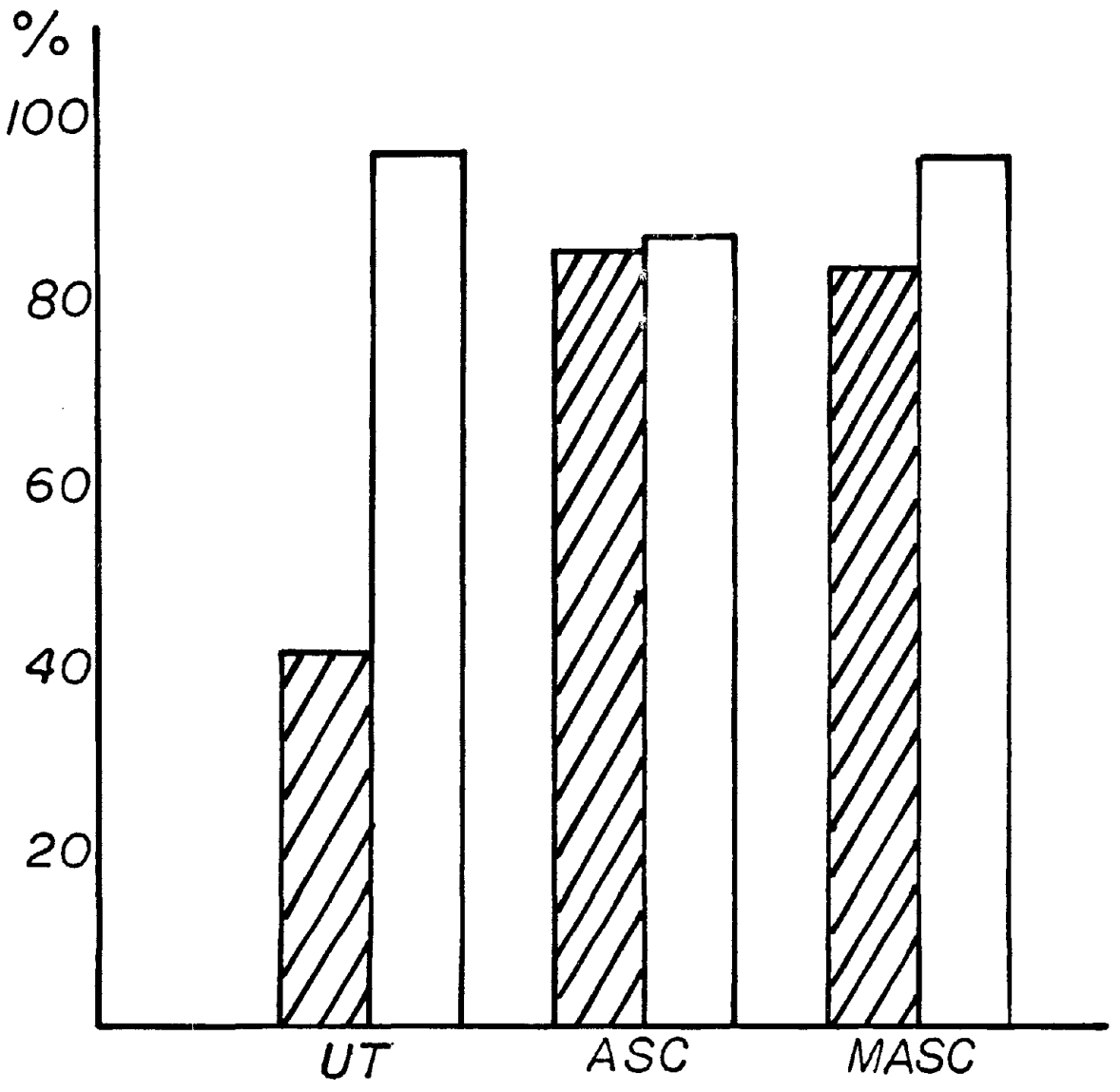

FIGURE 17. RESULTS OF RECOGNITION EXPERIMENT ON S6-8 USING ASC AND MASC TRANSFORMED F6-11 SIGNATURES. The striped bar is the percentage correct wheat while the open bar is the percentage other correct.

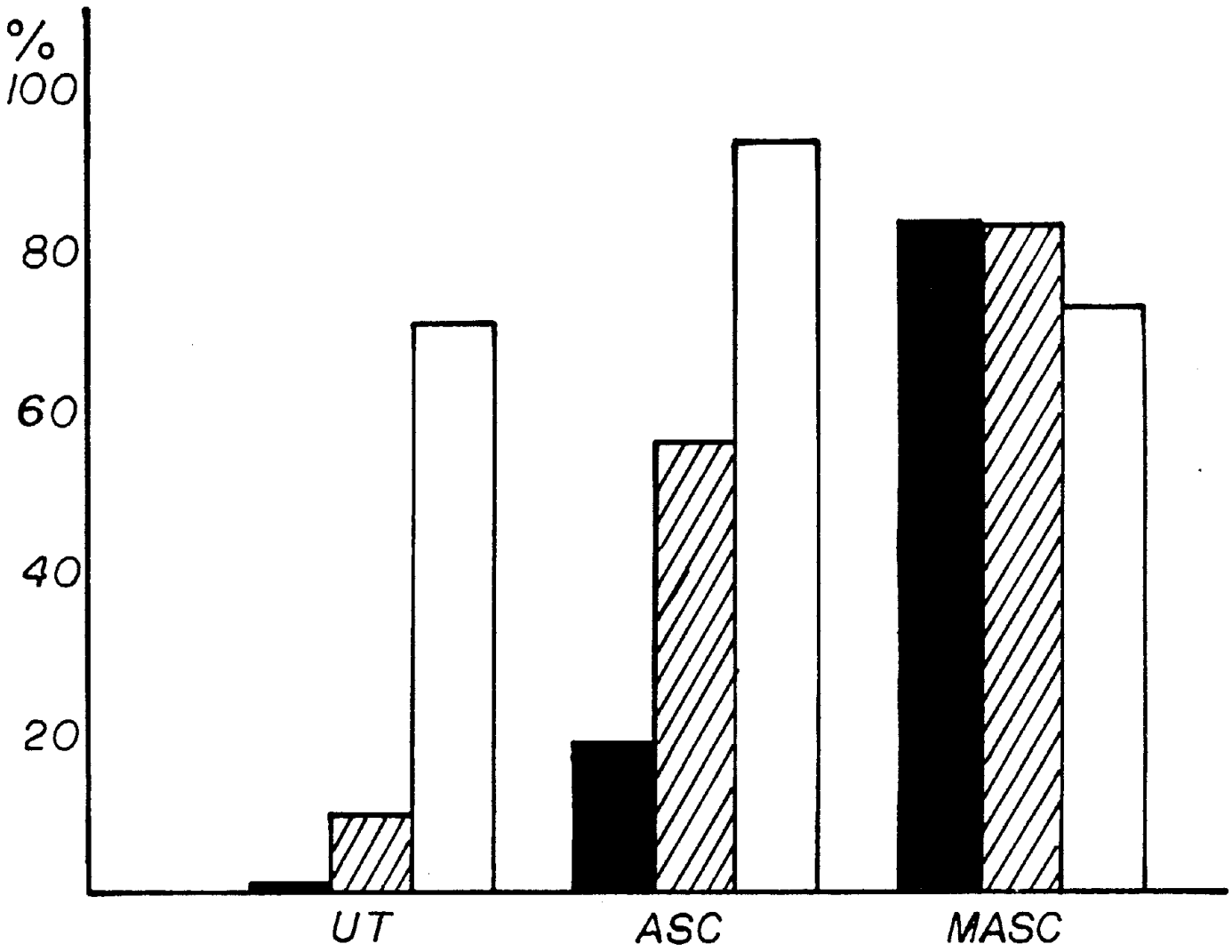

FIGURE 18. RESULTS OF RECOGNITION EXPERIMENT ON F8-21 USING ASC AND MASC TRANSFORMED W8-21 SIGNATURES. The solid bar is percentage correct corn recognition while the striped bar is percentage soy correct. The open bar is percentage other correct.

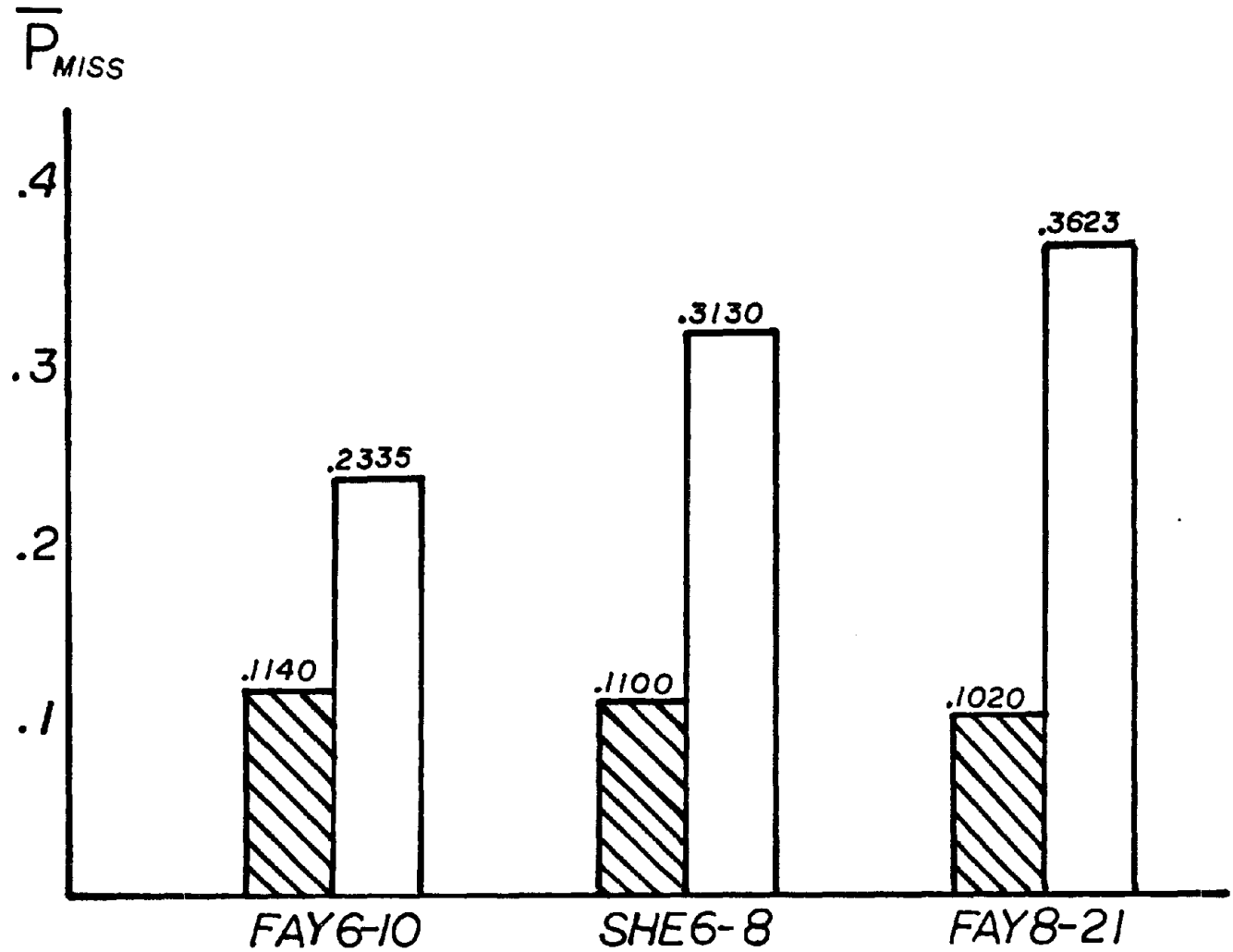

FIGURE 19 AVERAGE PROBABILITY OF MISCLASSIFICATION

(Striped bar is for MASC transformed signatures; Open bar is for untransformed signatures)

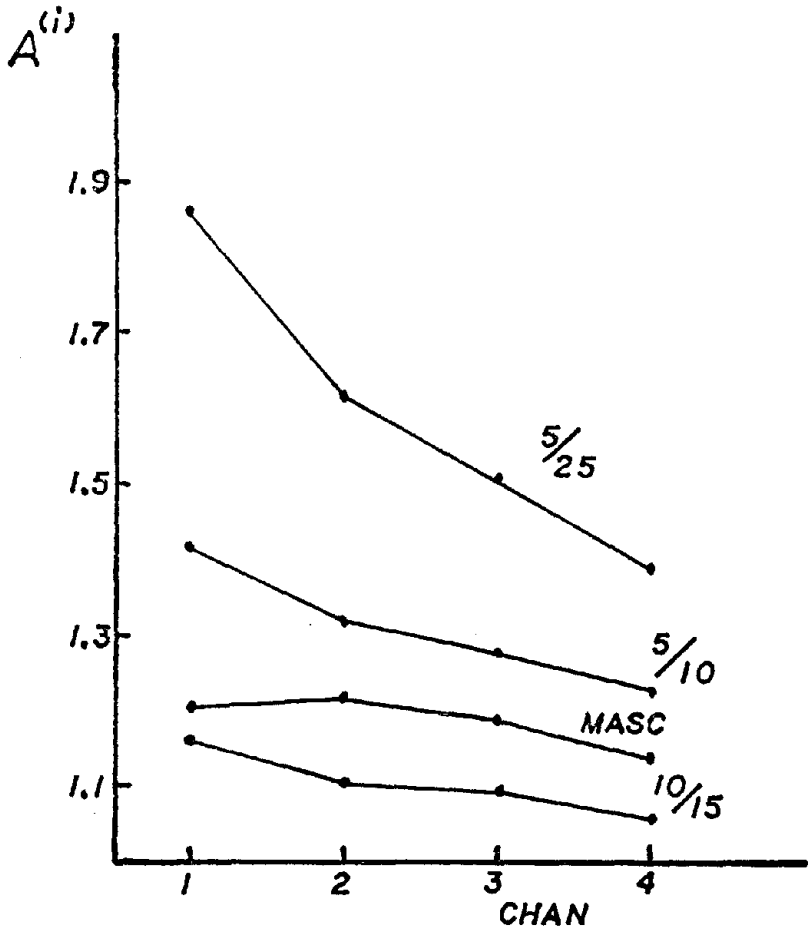

FIGURE 20. MULTIPLICATIVE SIGNATURE CORRECTION CALCULATED FROM ERIM RADIATIVE TRANSFER MODEL AND FROM MASC FOR THE TRANSFORMATION F6-11 → F6-10. Ratios are assumed visibility (km) for F6-11 to visibility for F6-10.

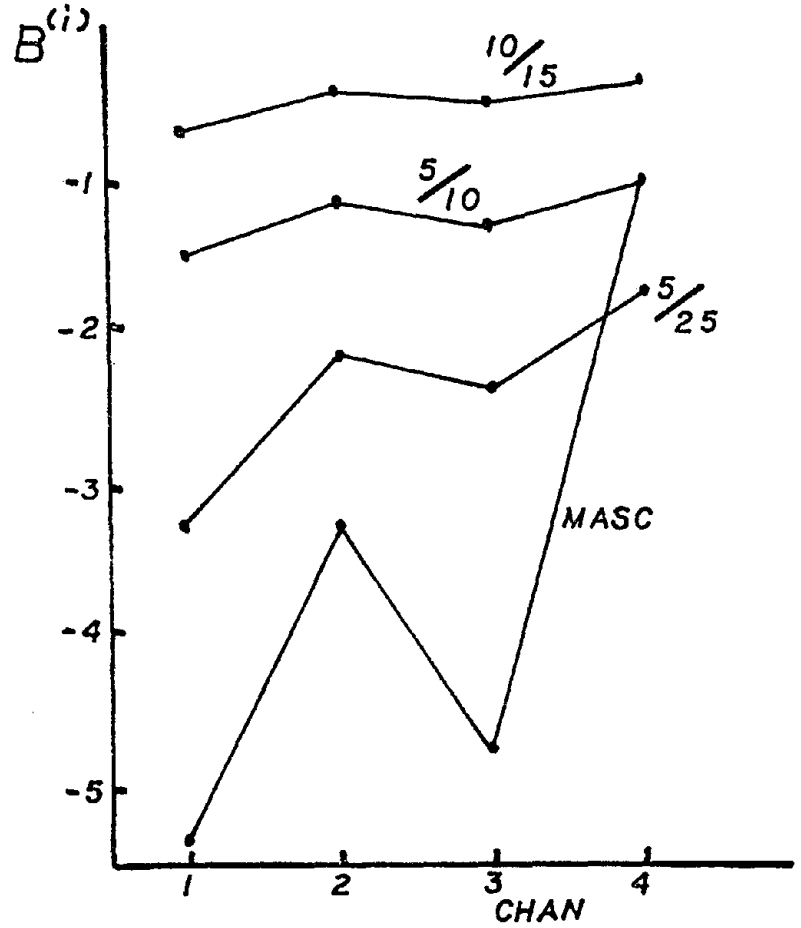

FIGURE 21. ADDITIVE SIGNATURE CORRECTION FOR F6-11 → F6-10

magnitude apparent in Fig. 21 may be due to not having the correct values of $A^{(i)}$ calculated by the model. This anomaly could very possibly be due to the fact that visibility was used as an input to the model rather than the more exact optical thickness. Also the model calculations are not exact since the parameter values at the middle of the LANDSAT-1 bands were used rather than integrating over the bands. More investigation into such questions as this may prove fruitful in the future.

It should be noted that none of the signature extension algorithms presented here should be considered to be in their final form. For instance, other methods of forming correspondences between clusters in the MASC algorithm are possible. When these methods are examined it may be possible to devise an improved version of MASC.

We have shown that similarities exist between cluster patterns based on spatially separated data sites . Two methods were described which allowed the cluster patterns from different data sets to be numerically compared. These methods were also used to transfer information between cluster patterns. The location of one object class was transferred between a pair of cluster patterns with reasonable results.

In the future recognition should be used to evaluate the accuracy of the methods used to map crop regions from one cluster pattern to another. In addition, phenological models of various vegetative spectral classes should be developed.

APPENDIX I: MASC ALGORITHM

We present here a step-by-step guide and flow chart for the MASC algorithm.

STEP 1. Both the extended from (Set 1) and extended to (set 2) data sets are input.

STEP 2. Unsupervised clustering is performed on both data sets. All input parameters to the cluster program should be the same for both data sets.

STEP 3. All clusters containing less than 1% of all pixels are removed from consideration.

STEP 4. After Step 3 above there are N_1 clusters from data set 1 and N_2 clusters from data set 2. The minimum of N_1 and N_2 is chosen so that a one-one correspondence between the two cluster sets is possible.

STEP 5. The channel containing the largest range of values is chosen for ordering clusters.

STEP 6. Both cluster sets are ordered on basis of their mean values in the above mentioned channel. The cluster in data set 1 with the largest mean in the selected channel is labeled number one, the cluster with the second largest mean is labeled number two, etc. The same ordering procedure is applied to data set 2. (Note: By cluster mean we intend the mean of the Gaussian distribution which represents the cluster.)

STEP 7. A one-to-one correspondence is formed between the first N clusters of the data sets ($N = \min(N_1, N_2)$). The means of the corresponded clusters define points in two space.

STEP 8. Regression is used with the set of points from Step 7 to yield the parameters to the equation

$$C_2^{(i)} = A^{(i)} C_1^{(i)} + B^{(i)},$$

where the subscripts represent data sets 1 and 2.

STEPS 9 and 10. Any points whose percentage deviation, in any channel, from the line of equation (1) is greater than 10% are removed and regression is re-entered.

STEP 11. The parameters $A^{(i)}$ and $B^{(i)}$ which result from the regression are used as multiplicative ($A^{(i)}$) and additive ($B^{(i)}$) signature corrections for the signatures from data set 1. Thus the signatures from data set 1 can be extended to data set 2.

MASC ALGORITHM

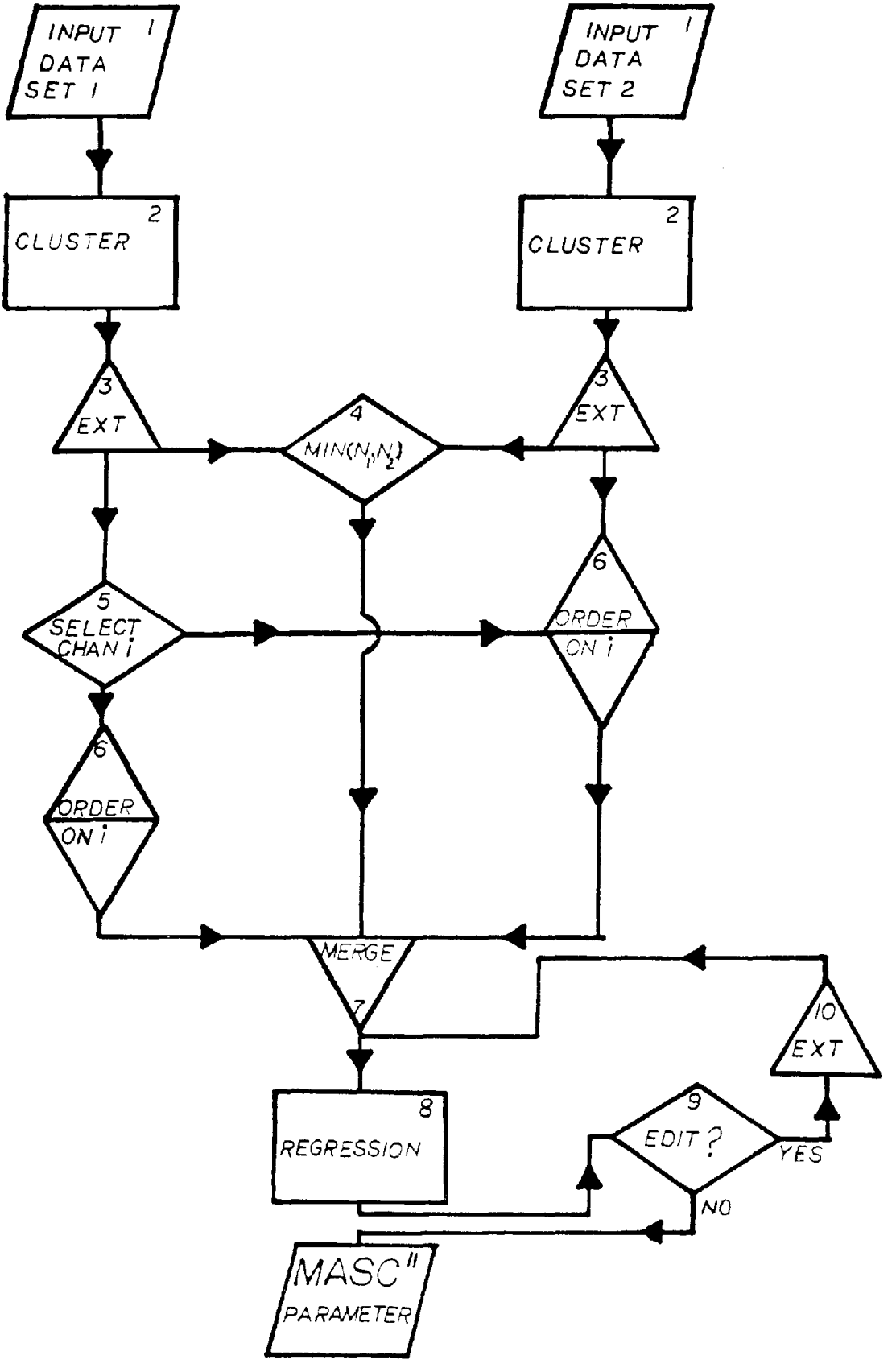

APPENDIX II

MASC PARAMETERS

The multiplicative, $A^{(i)}$, and additive, $B^{(i)}$, MASC parameters used on the CITARS data sets are listed in Table A1 below.

TABLE A1. MASC PARAMETERS USED FOR TDS TO RDS TRANSFORMATIONS

Training Data Set	Recognition Data Set	Channel (i)	$A^{(i)}$	$B^{(i)}$
Fayette June 11	Fayette June 10	1	1.201	-5.308
		2	1.212	-3.242
		3	1.185	-4.729
		4	1.139	- .997
	Shelby June 8	1	.794	8.665
		2	.902	3.575
		3	.652	17.711
		4	.605	9.688
White August 21	Fayette August 21	1	2.15	-22.449
		2	2.23	-12.841
		3	.78	13.156
		4	.87	2.488

APPENDIX III

GENERAL CLUSTER PATTERNS FOR AGRICULTURAL SCENES

In order to achieve a better understanding of just what is portrayed in the cluster patterns and why a general or 'complete' cluster pattern has the shape it does, ERIM's vegetative canopy model [10] was called into play. As it happened, the necessary model inputs for a certain type of vegetation, Ionia wheat (a variety grown in Michigan) were readily available. And so, two soil reflectances were selected, one to simulate a darker, perhaps more organic or moist soil and the other to simulate a lighter colored, perhaps sandier or drier soil (for more information of the importance of soil moisture on soil reflectance, see Blanchard et al., 1974 [11] and Parks et al., 1974 [12]) and a construction made of the phenology of a sample of wheat, Ionia variety with two very different soil backgrounds (See Figure A1). As may be seen, the soil background plays a dominant role in the bidirectional reflectance of a stand of Ionia wheat until the onset of plant maturity. If the bare soil points are connected by a line, hereafter called the bare soil line, the outline of the phenology of Ionia wheat is very similar to the outline of the 'complete' cluster pattern. It is not unreasonable to suspect, therefore, that location within a cluster pattern represents, to a degree, vegetative state of development as modified by such factors as soil reflectance, stress of various kinds, mixtures of vegetation and so on. As an actual example

---

[10] G. Suits, "The Calculation of the Directional Reflectance of a Vegetative Canopy", Remote Sensing of Environment, V. 2, 1972, pp. 117-125.

[11] M. B. Blanchard, R. Greeley and R. Goettelman, "Use of Visible, Near-Infrared, and Thermal Infrared Remote Sensing to Study Soil Moisture", Proceedings of Ninth International Symposium on Remote Sensing of Environment, Ann Arbor, Michigan, April 1974.

[12] W. L. Parks, J. I. Sewell, J. W. Hilty and J. C. Rennie, "Utilizing ERTS Imagery to Detect Plant Diseases and Nutrient Deficiencies, Soil Types and Soil Moisture Levels", Report No. NAS5-21873, NASA/GSFC, March 1974.

FIGURE A1. PHENOLOGY FOR WHEAT (IONIA VARIETY) BASED ON CANOPY MODEL

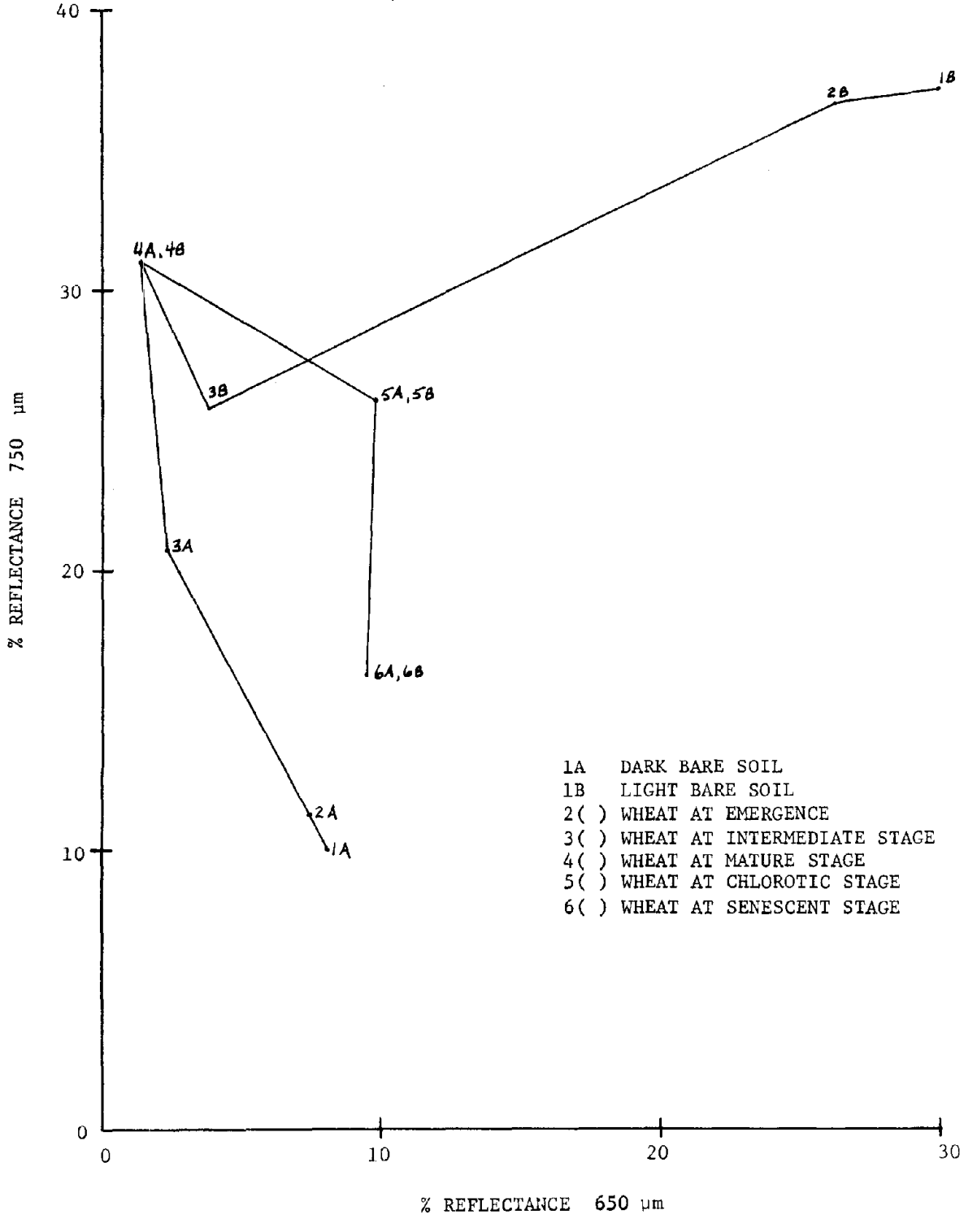

of the extreme variability present in the reflectance characteristics of a crop such as soybeans (varieties unknown) at the emergence stage see the cluster plots for soybeans based on the Fayette 16 July and Livingston 16 July data sets (Figures A2 through A5). By overlaying the Fayette soybean cluster plot (Figure A2) onto the cluster plot based on Fayette quarter sections (Figure A3) the fact emerges that soybeans in Fayette Co. were planted in soils on the upper (brighter) half of the bare soil line. When one follows the same procedure for Livingston Co. (Figures A4 and A5 respectively) one sees that soybeans were planted in soils on the lower (darker) half of the bare soil line. The important soybean clusters (with most of the points) are 1, 2, 3, 5 and 8 for Fayette Co. and 1, 2, 3, 4, 5 and 7 for Livingston Co. Analysis of a time sequence of plots such as these for a variety of vegetative types can aid in predicting where in the cluster pattern a certain crop should be (allowing for the sources of variability discussed previously) at a certain point in its crop calendar.

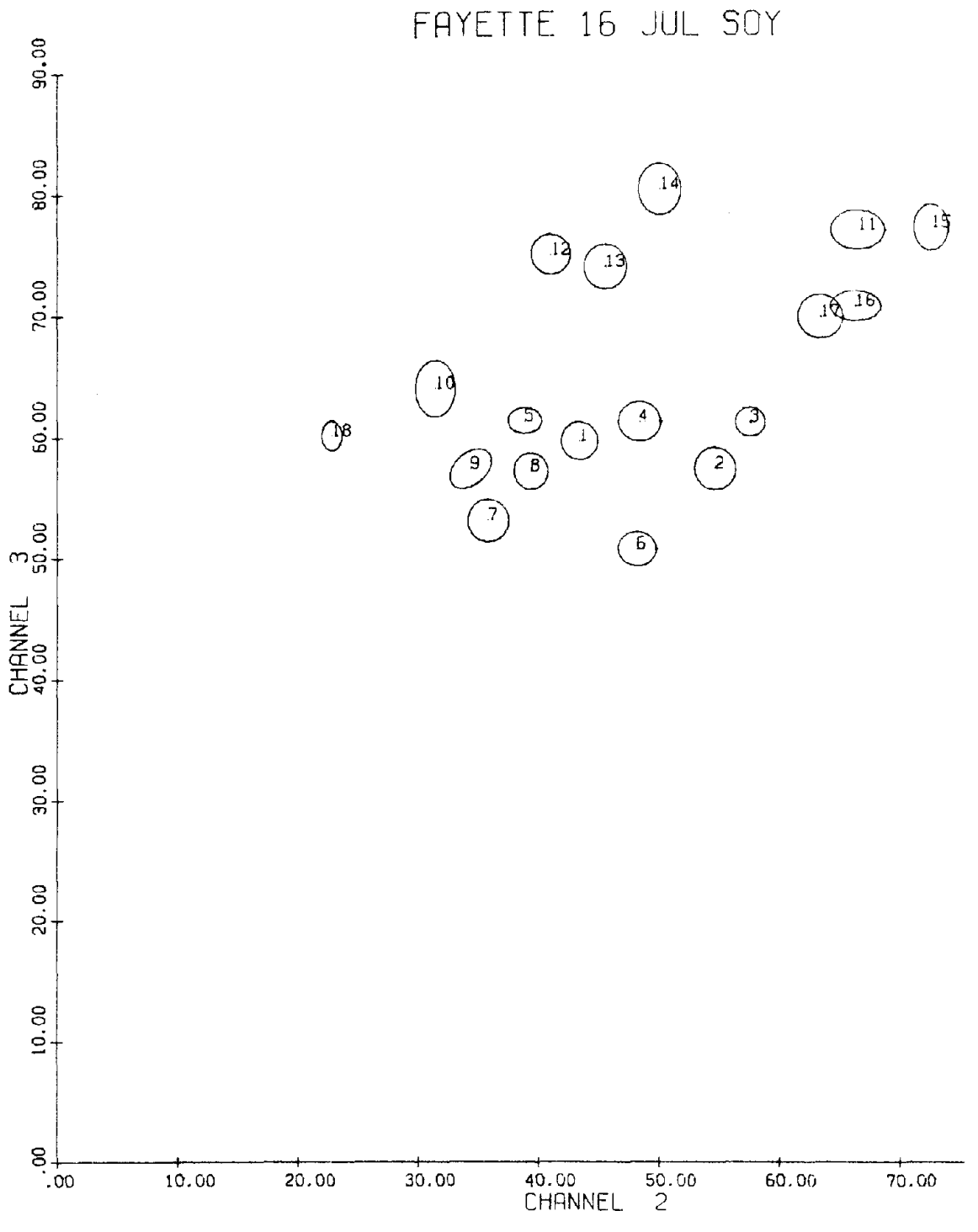

FIGURE A2. SOY CLUSTERS FROM FAYETTE 16 JULY

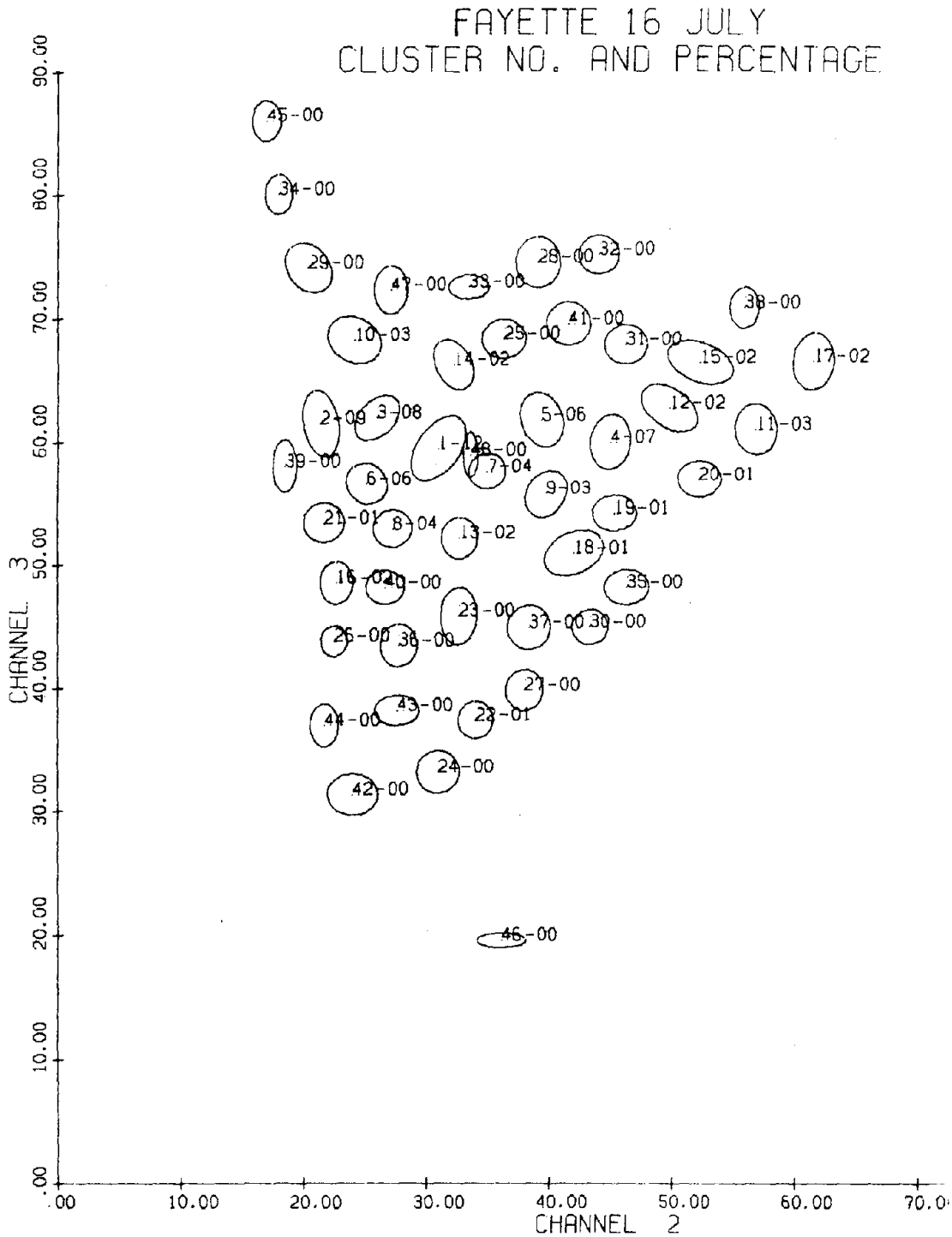

FIGURE A3. GENERAL CLUSTER PATTERN FOR FAYETTE 16 JULY

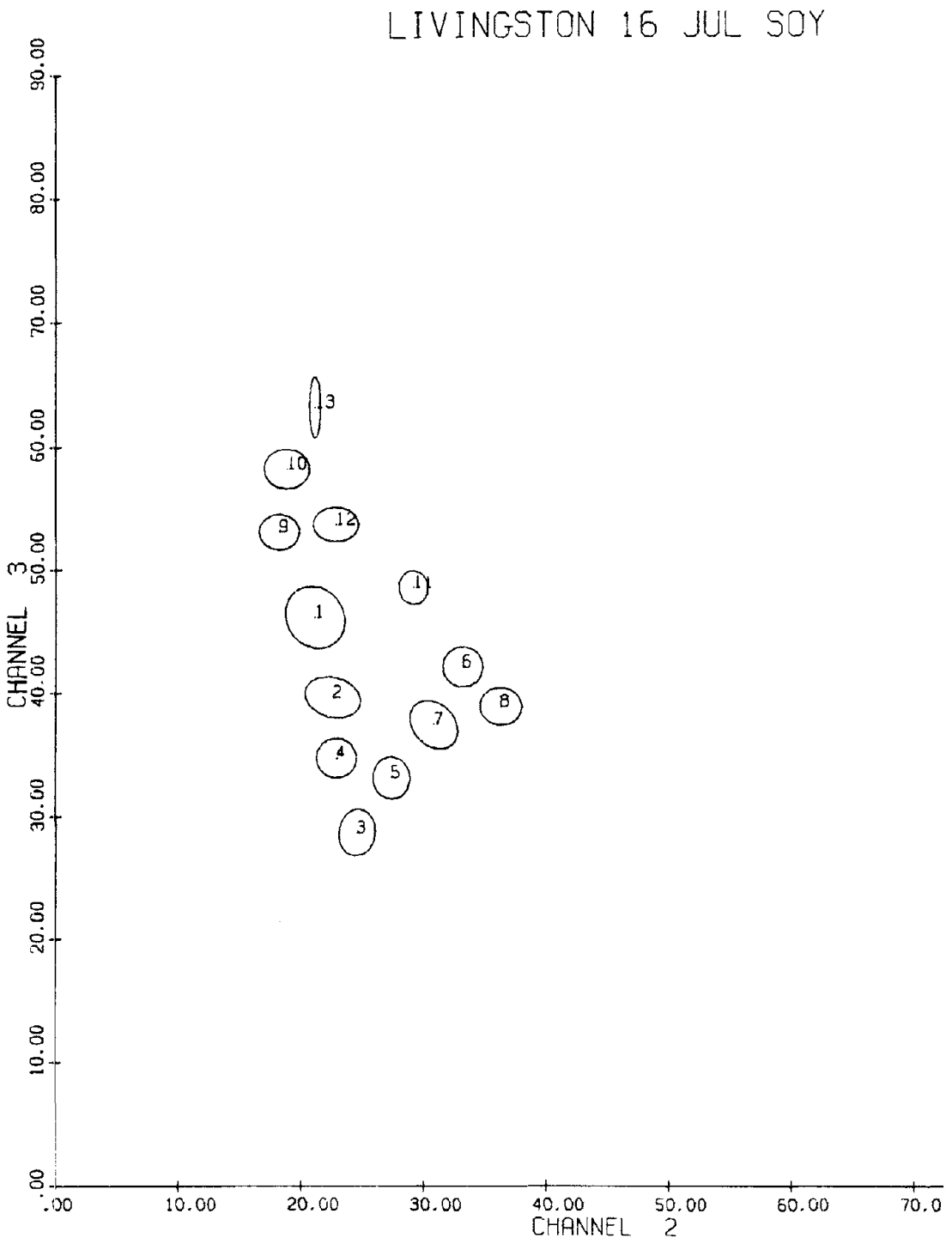

FIGURE A4. SOY CLUSTERS FROM LIVINGSTON 16 JULY

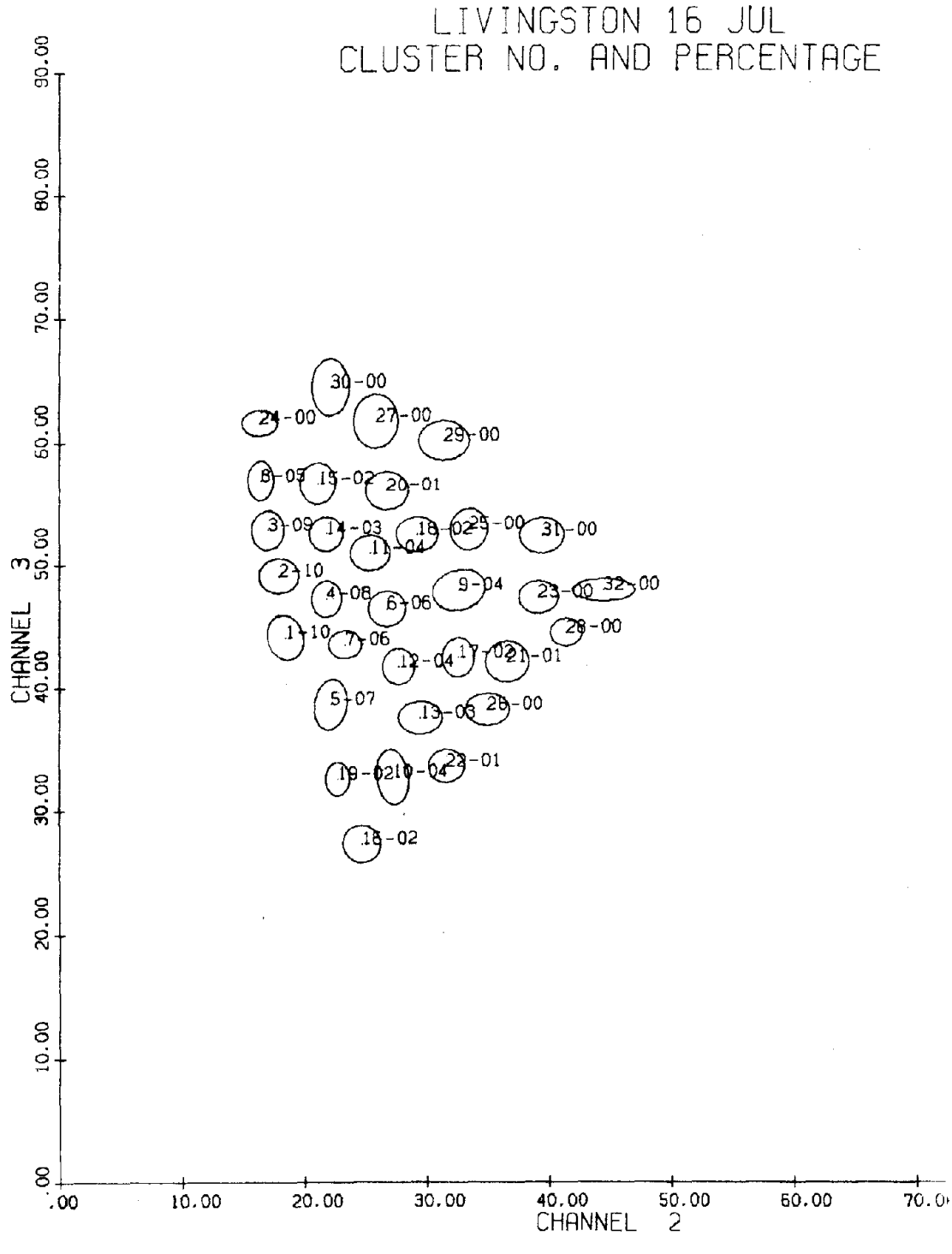

FIGURE A5. GENERAL CLUSTER PATTERN FOR LIVINGSTON 16 JULY

APPENDIX IV

ABBREVIATIONS USED IN THIS REPORT

ASC - Additive Signature Correction

MASC - Multiplicative and Additive Signature Correction

MAT - Method of Affine Transformations

MLA - Mean Level Adjustment

MSS - Multispectral Scanner

RADIFF - Ratio of Differences in Spectral Bands

Ratio - Ratio of Spectral Bands

RDS - Recognition Data Set

TDS - Training Data Set

Data Sets

F6-10 - Fayette Co., Illinois, June 10, 1973

F6-11 - Fayette Co., Illinois, June 11, 1973

S6-8 - Shelby Co., Indiana, June 8, 1973

F8-21 - Fayette Co., Illinois, August 21, 1973

W8-21 - White Co., Indiana, August 21, 1973

REFERENCES

1. Robert E. Turner, "Radiative Transfer in Real Atmospheres", ERIM Report No. 190100-24-T, December 1973.

2. W. A. Malila, D. P. Rice and R. C. Cicone, "Final Report on the CITARS Effort by the Environmental Research Institute of Michigan", ERIM Report No. 109600-12-F, February 1975.

3. R. B. Crane, W. Richardson, R. H. Hieber and W. A. Malila, "A Study of Techniques for Processing Multispectral Scanner Data", ERIM Report No. 31650-155-T, September 1973.

4. H. M. Horwitz, J. T. Lewis and A. P. Pentland, "Estimating Proportions of Objects From Multispectral Scanner Data", ERIM Report No. 109600-13-F, April 1975, Section 4.4 and Appendix E.

5. R. K. Vincent, G. S. Thomas and R. F. Nalepka, "Signature Extension Studies", ERIM Report No. 190100-26-T, July 1974.

6. R. F. Nalepka and J. P. Morgenstern, "Signature Extension: An Approach to Operational Multispectral Surveys", ERIM Report No. 31650-152-T, March 1973.

7. Ibid., p. 36.

8. ERTS Data Users Handbook, NASA Document No. 71SD4249, Appendix G.

9. Personal communication from R. M. Bizzell.

10. G. Suits, "The Calculation of the Directional Reflectance of a Vegetative Canopy", Remote Sensing of Environment, V. 2, 1972, pp. 117-125.

11. M. B. Blanchard, R. Greeley and R. Goettelman, "Use of Visible, Near-Infrared, and Thermal Infrared Remote Sensing to Study Soil Moisture", Proceedings of Ninth International Symposium on Remote Sensing of Environment, Ann Arbor, Michigan, April 1974.

12. W. L. Parks, J. I. Sewell, J. W. Hilty and J. C. Rennie, "Utilizing ERTS Imagery to Detect Plant Diseases and Nutrient Deficiencies, Soil Types and Soil Moisture Levels", Report No. NAS5-21873, NASA/GSFC, March 1974.

Technical and Final Report Distribution List

NASA Contract NAS9-14123

Tasks II thru X

NAME	NUMBER OF COPIES
NASA/Johnson Space Center Earth Observations Division Houston, Texas 77058	
ATTN: Mr. Robert MacDonald/TF	(1)
ATTN: Mr. B. Erb/TF2	(1)
ATTN: Dr. F. Hall/TF2	(1)
ATTN: Mr. J. Murphy/TF2	(1)
ATTN: Dr. A. Potter/TF3	(8)
ATTN: Mr. J. Dragg/TF4	(1)
ATTN: Earth Resources Data Facility/TF12	(8)
NASA/Johnson Space Center Earth Resources Program Office Office of the Program Manager Houston, Texas 77058	
ATTN: Mr. Clifford E. Charlesworth/HA	(1)
ATTN: Mr. William E. Rice/HA	(1)
NASA/Johnson Space Center Earth Resources Program Office Program Analysis & Planning Office Houston, Texas 77058	
ATTN: Dr. O. Glenn Smith/HD	(1)
NASA/Johnson Space Center Earth Resources Program Office Systems Analysis and Integration Office Houston, Texas 77058	
ATTN: Mr. Richard A. Moke/HC	(1)
ATTN: Mr. M. Jay Harnage, Jr./HC	(1)
NASA/Johnson Space Center Technical Library Branch Houston, Texas 77058	
ATTN: Ms. Retha Shirkey/JM6	(4)

NAME	NUMBER OF COPIES
NASA/Johnson Space Center Management Services Division Houston, Texas 77058 ATTN: Mr. John T. Wheeler/AT3	(1)
NASA/Johnson Space Center Technical Support Procurement Houston, Texas 77058 ATTN: Mr. J. Haptonstall/BB63	(1)
Earth Resources Laboratory, GS Mississippi Test Facility Bay St. Louis, Mississippi 39520 ATTN: Mr. D. W. Mooneyhan	(1)
EROS Data Center U.S. Department of Interior Sioux Falls, South Dakota 57198 ATTN: Mr. G. Thorley	(1)
Department of Mathematics Texas A&M University College Station, Texas 77843 ATTN: Dr. Larry Guseman	(1)
NASA/Johnson Space Center Computation & Flight Support Houston, Texas 77058 ATTN: Mr. Eugene Davis/FA	(1)
U.S. Department of Agriculture Agricultural Research Service Washington, D.C. 20242 ATTN: Dr. Robert Miller	(1)
U.S. Department of Agriculture Soil & Water Conservation Research Division P.O. Box 267 Weslaco, Texas 78596 ATTN: Dr. Craig Wiegand	(1)

NAME	NUMBER OF COPIES
U.S. Department of Interior Geology Survey Washington, D.C. 20244 ATTN: Dr. James R. Anderson	(1)
Director, Remote Sensing Institute South Dakota State University Agriculture Engineering Building Brookings, South Dakota 57006 ATTN: Mr. Victor I. Myers	(1)
U.S. Department of Interior Fish & Wildlife Service Bureau of Sport Fisheries & Wildlife Northern Prairie Wildlife Research Center Jamestown, North Dakota 58401 ATTN: Mr. Harvey K. Nelson	(1)
U.S. Department of Agriculture Forest Service 240 W. Prospect Street Fort Collins, Colorado 80521 ATTN: Dr. Richard Driscoll	(1)
U.S. Department of Interior Geological Survey Water Resources Division 500 Zack Street Tampa, Florida 33602 ATTN: Mr. A.E. Coker	(1)
U.S. Department of Interior Director, EROS Program Washington, DC 20244 ATTN: Mr. J. M. Denoyer	(1)
U.S. Department of Interior Geological Survey GSA Building, Room 5213 Washington, DC 20242 ATTN: Mr. W.A. Fischer	(1)

NAME	NUMBER OF COPIES
NASA Wallops Wallops Station, Virginia 23337	
ATTN: Mr. James Bettle	(1)
Purdue University Purdue Industrial Research Park 1200 Potter Drive West Lafayette, Indiana 47906	
ATTN: Dr. David Landgrebe	(1)
ATTN: Dr. Philip Swain	(1)
ATTN: Mr. Terry Phillips	(1)
U.S. Department of Interior EROS Office Washington, DC 20242	
ATTN: Dr. Raymond W. Fary	(1)
U.S. Department of Interior Geological Survey 801 19th Street, N.W. Washington, DC 20242	
ATTN: Mr. Charles Withington	(1)
U.S. Department of Interior Geological Survey 801 19th Street, N.W. Washington, DC 20242	
ATTN: Mr. M. Deutsch	(1)
U.S. Geological Survey 801 19th Street, N.W., Room 1030 Washington, DC 20242	
ATTN: Dr. Jules D. Friedman	(1)
U.S. Department of Interior Geological Survey Federal Center Denver, Colorado 80225	
ATTN: Dr. Harry W. Smedes	(1)

NAME	NUMBER OF COPIES
U.S. Department of Interior Geological Survey Water Resources Division 901 S. Miami Ave. Miami, Florida 33130 ATTN: Mr. Aaron L. Higer	(1)
University of California School of Forestry Berkeley, California 94720 ATTN: Dr. Robert Colwell	(1)
School of Agriculture Range Management Oregon State University Corvallis, Oregon 97331 ATTN: Dr. Charles E. Poulton	(1)
U.S. Department of Interior EROS Office Washington, DC 20242 ATTN: Mr. William Hemphill	(1)
Chief of Technical Support Western Environmental Research Laboratories Environmental Protection Agency P.O. Box 15027 Las Vegas, Nevada 89114 ATTN: Mr. Leslie Dunn	(1)
NASA/Langley Research Mail Stop 470 Hampton, Virginia 23365 ATTN: Mr. William Howle	(1)
U.S. Geological Survey Branch of Regional Geophysics Denver Federal Center, Building 25 Denver, Colorado 80225 ATTN: Mr. Kenneth Watson	(1)

NAME	NUMBER OF COPIES
NAVOCEANO, Code 7001 Naval Research Laboratory Washington, DC 20390 ATTN: Mr. J. W. Sherman, III	(1)
U.S. Department of Agriculture Administrator Agricultural Stabilization and Conservation Service Washington, DC ATTN: Mr. Kenneth Frick	(1)
Pacific Southwest Forest & Range Experiment Station U.S. Forest Service P. O. Box 245 Berkeley, CA 94701 ATTN: Mr. R. C. Heller	(1)
United States Department of Agriculture/Forestry Service Division of Forest Economics and Marketing Resources 1200 Independence Avenue Washington, D.C. 20250 ATTN: Dr. P. Weber	(1)
University of Texas at Dallas Box 688 Richardson, Texas 75080 ATTN: Dr. Patrick L. Odell	(1)
Department of Mathematics University of Houston Houston, Texas 77004 ATTN: Dr. Henry Decell	(1)
Institute for Computer Services and Applications Rice University Houston, Texas 77001 ATTN: Dr. M. Stuart Lynn	(1)

NAME	NUMBER OF COPIES
U.S. National Park Service Western Regional Office 450 Golden Gate Avenue San Francisco, California 94102 ATTN: Mr. M. Kolipinski	(1)
U.S. Department of Agriculture Statistical Reporting Service Washington, DC 20250 ATTN: D. H. VonSteen/R. Allen	(2)
U.S. Department of Agriculture Statistical Reporting Service Washington, DC 20250 ATTN: Mr. H. L. Trelogan, Administrator	(1)
Department of Watershed Sciences Colorado State University Fort Collins, Colorado 80521 ATTEN: Dr. James A. Smith	(1)
Lockheed Electronics Co. 16811 El Camino Real Houston, Texas 77058 ATTN: Mr. R. Tøkerud	(1)
TRW System Group Space Park Drive Houston, Texas 77058 ATTN: Dr. David Detchmendy	(1)
IBM Corporation 1322 Space Park Drive Houston, Texas 77058 ATTN: Dr. D. Ingram	(1)
S&D - DIR Marshall Space Flight Center Huntsville, Alabama 35812 ATTN: Mr. Cecil Messer	(1)

NAME	NUMBER OF COPIES
Code 168-427 Jet Propulsion Laboratory 4800 Oak Grove Drive Pasadena, California 91103	
ATTN: Mr. Fred Billingsley	(1)
NASA Headquarters Washington, DC 20546	
ATTN: Mr. W. Stoney/ER	(1)
ATTN: Mr. Leonard Jaffe/ER	(1)
ATTN: Mr. M. Molloy/ERR	(1)
ATTN: Mr. James R. Morrison	(1)
Ames Research Center National Aeronautics and Space Administration Moffett Field, California 94035	
ATTN: Dr. D. M. Deerwester	(1)
Goddard Space Flight Center National Aeronautics and Space Administration Greenbelt, Maryland 20771	
ATTN: Mr. W. Nordberg, 620	(1)
ATTN: Mr. W. Alford, 563	(1)
Lewis Research Center National Aeronautics and Space Administration 21000 Brookpark Road Cleveland, Ohio 44135	
ATTN: Dr. Herman Mark	(1)
John F. Kennedy Space Center National Aeronautics and Space Administration Kennedy Space Center, Florida 32899	
ATTN: Mr. S. Claybourne/FP	(1)
NASA/Langley Mail Stop 214 Hampton, Virginia 23665	
ATTN: Mr. James L. Raper	(1)

NAME	NUMBER OF COPIES
Texas A&M University Institute of Statistics College Station, TX 77843	
ATTN: Dr. H. O. Hartley	(1)
Texas Tech University Department of Mathematics P. O. Box 4319 Lubbock, TX 79404	
ATTN: Dr. T. Boullion	(1)
Mr. James D. Nichols Space Sciences Laboratory, Rm. 260 University of California Berkeley, CA 94720	(1)
EXXON Production Research Co. P. O. Box 2189 Houston, TX 77001	
ATTN: Mr. J. O. Bennett	(1)